AD-A101 010   LITTON SYSTEMS INC   WOODLAND HILLS CA GUIDANCE AND CO--ETC F/G 7/4
              NUCLEAR MOMENT ALIGNMENT, RELAXATION AND DETECTION MECHANISMS.(U)
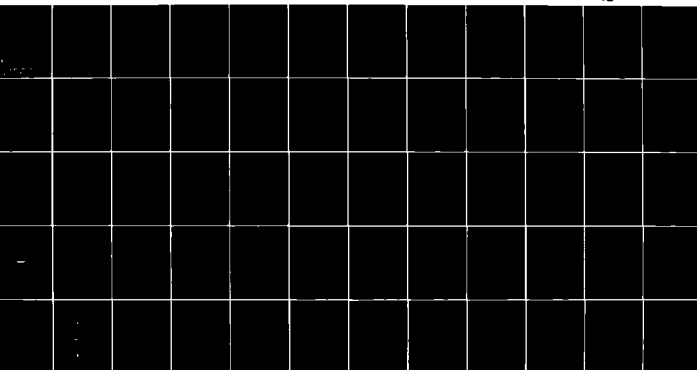   FEB 81   T M KWON   F49620-77-C-0047
UNCLASSIFIED 404577   AFOSR-TR-81-0503   NL

AD
A101010

END
DATE
FILMED
7-81
DTIC

AFOSR-TR- 81-0503

Document No. 404577

LEVEL

$A081880$

AD A101010

NUCLEAR MOMENT ALIGNMENT, RELAXATION
AND DETECTION MECHANISMS

February 1980 - January 1981

ANNUAL TECHNICAL REPORT

Contract No. F49620-77-C-0047 ✓

Prepared for

AIR FORCE OFFICE OF SCIENTIFIC RESEARCH

DTIC FILE COPY

**DTIC
ELECTE
JUL 7 1981**

A

GUIDANCE & CONTROL SYSTEMS
Litton 5500 Canoga Avenue, Woodland Hills, California 91365

81 7 06 118

REPORT DOCUMENTATION PAGE		READ INSTRUCTIONS BEFORE COMPLETING FORM
1. REPORT NUMBER AFOSR-TR- 81-0503	2. GOVT ACCESSION NO. AD-A101 010	3. RECIPIENT'S CATALOG NUMBER
4. TITLE (and Subtitle) NUCLEAR MOMENT ALIGNMENT, RELAXATION AND DETECTION MECHANISMS		5. TYPE OF REPORT & PERIOD COVERED Annual (February 1980 January 1981)
		6. PERFORMING ORG. REPORT NUMBER 404577
7. AUTHOR(s) Tae M. Kwon		8. CONTRACT OR GRANT NUMBER(s) F49620-77-C-0047
9. PERFORMING ORGANIZATION NAME AND ADDRESS Litton Guidance & Control Systems 5500 Canoga Ave. Woodland Hills, CA. 91365		10. PROGRAM ELEMENT, PROJECT, TASK AREA & WORK UNIT NUMBERS 61102F 2301/A4
11. CONTROLLING OFFICE NAME AND ADDRESS Director of Physics Air Force Office of Scientific Research Attn: NP Building 410, Bolling AFB, D.C. 20332		12. REPORT DATE February 1981
		13. NUMBER OF PAGES 66
14. MONITORING AGENCY NAME & ADDRESS(if different from Controlling Office)		15. SECURITY CLASS. (of this report) UNCLASSIFIED
		15a. DECLASSIFICATION/DOWNGRADING SCHEDULE

16. DISTRIBUTION STATEMENT (of this Report)

Approved for public release; distribution unlimited.

17. DISTRIBUTION STATEMENT (of the abstract entered in Block 20, if different from Report)

18. SUPPLEMENTARY NOTES

19. KEY WORDS (Continue on reverse side if necessary and identify by block number)

Nuclear Magnetic Resonance	Nuclear Moment Relaxation	Frequency Shift
Gyroscope	Quadrupole Relaxation	
Optical Pumping	Nuclear Moment Precession	
Nuclear Moment Alignment	Spin Exchange	

20. ABSTRACT (Continue on reverse side if necessary and identify by block number)

The reported physics research is part of an overall program to develop a nuclear magnetic resonance gyro that makes use of an optically pumped alkali metal vapor both to align the magnetic moments of the noble gas nuclei and to detect the weak magnetic fields that are generated by these precessing nuclear moments.

Theoretical and experimental investigations are reported on the relaxation of polarized nuclear spins of Xe^{131} through the interaction of the nuclear quadrupole moment with the electric field gradient. The field gradient arises from deformation of the otherwise spherical electronic shell of the zenon

DD FORM 1473 EDITION OF 1 NOV 65 IS OBSOLETE

NUCLEAR MOMENT ALIGNMENT, RELAXATION

AND DETECTION MECHANISMS

February 1980 - January 1981

ANNUAL TECHNICAL REPORT

Prepared for

AIR FORCE OFFICE OF SCIENTIFIC RESEARCH

Under

Contract No. F49620-77-C-0047

Approved By:

Emery L. Moore

Emery L. Moore
Manager, NMR Gyro Project

GUIDANCE & CONTROL SYSTEMS
Litton 5500 Canoga Avenue, Woodland Hills, California 91365

404577

TABLE OF CONTENTS

i

404577

LIST OF ILLUSTRATIONS

404577

SECTION I

PROGRAM DESCRIPTION

1.1 INTRODUCTION

The Guidance and Control Systems Division of Litton Systems, Inc. is involved in a multi-year program in the research and development of a nuclear magnetic resonance (NMR) gyro for use in inertial navigation systems.

In the magnetic resonance gyro, angular craft rate is sensed through a shift in the precession frequency of an ensemble of atomic or nuclear magnetic moments. The Litton NMR gyro utilizes ensembles of two noble gas isotopes in order to eliminate explicit dependence on the magnetic field. In order to obtain the gyroscopic information in this scheme, the noble gas ensembles must first be polarized so that coherent precession about an applied magnetic field can take place and, secondly, a means for detecting the nuclear precession must be provided. In the Litton approach, the noble gas ensembles attain a net magnetic moment through spin exchange with an optically oriented alkali vapor. In addition, the alkali vapor, through a magnetometer effect, detects the weak magnetic fields, which are generated by the precessing nuclear moments of the two noble gases, and thus provides the gyro angular rate information.

The purpose of the physics research program is to develop a stronger theoretical and empirical understanding of the alkali-atom noble-gas-atom system. Of particular interest are the spin exchange interactions between the alkali valence electrons and the noble gas nuclei, the noble gas nuclear spin relaxation mechanisms as they pertain to the NMR gyro and other related phenomena which impact the NMR gyro technology.

1.2 OBJECTIVES AND STATUS OF THE CURRENT PROGRAM

The research tasks described in Sections II and III of this
report are part of our continuing effort to understand and param-
eterize the alkali-atom noble-gas-nucleus spin exchange inter-
action. In addition, investigations of the spin exchange process
also provide opportunities to study the pertinent relaxation
mechanisms of the noble gas nuclei.

Reported in Section II are the results of the theoretical and
experimental investigation on the relaxation of polarized noble
gas nuclei through the interaction of the nuclear quadrupole
moment with the electric field gradient arising from collisions
with the walls. In the last AFOSR annual Technical Report, a
simple theoretical model of this effect was developed and was in
agreement with the experimental data only qualitatively. No
quantitative analysis of the data was possible with the model.
In the present work, the model has been extended to incorporate
the second order expansion of the nuclear density matrix. Under
this new model, measurements of the relaxation of Xe^{131} nuclei
were analyzed quantitatively, and, as a result, the sticking time
of the Xe^{131} atom onto the container wall and the strength of
the nuclear quadrupole interaction have been estimated for the
first time.

In Section III, we report on our measurement of the shift in the
Larmor precession frequency of the noble gas nuclei during spin
exchange with an optically oriented alkali vapor. The results
confirm that, for a given alkali polarization environment, the
difference in frequency shifts for different isotopes of the
same noble gas atom, such as Xe^{129} and Xe^{131}, is smaller by, at
least, an order of magnitude than the difference in frequency

shifts for different noble gas species, such as Xe^{129} and Kr^{83}. Experimental results are presented in terms of the parameters relevant to the NMR gyro.

Investigations into this area of physics have relevance not only to NMR gyro research but also to other possible areas of research such as magnetometers, atomic clocks, masers, laser stabilization, and polarized nuclear targets. It was in this light that the result of the work reported in Section II has been prepared as a scientific paper to be submitted for publication to The Physical Review. The preprint of this paper is included as paragraph 2.2.

In the course of this work, an idea was conceived to coat the container wall with RbH to reduce the nuclear quadrupole interaction. Successful implementation of the idea has been demonstrated in the data reported in Section II. We believe that the invention of the coating material and coating technique is a significant step forward in the development of NMR devices. It is for this reason that we have submitted a written disclosure of invention to the company for consideration in applying for a patent. The patent application is under consideration for further action by the corporate headquarters.

1.3 PROFESSIONAL PERSONNEL ASSOCIATED WITH THE PROGRAM

The principal investigator of these research efforts has been Dr. Tae M. Kwon. This work has also been strongly supported by Dr. Charles H. Volk, and Dr. John G. Mark. We also wish to acknowledge the contribution of Mr. Howard E. Williams for the design and Mr. William P. Debley for the construction of various components of the apparatus, including the resonance cells and lamps used in this research effort. Finally we acknowledge Dr. Edward Kanegsberg for many helpful discussions.

SECTION II

QUADRUPOLAR NUCLEAR SPIN RELAXATION

2.1 INTRODUCTION

Two nuclear species, Xe^{129} (I=1/2) and Xe^{131} (I=3/2), or Xe^{129} and Kr^{83} (I=9/2) are required under Litton's approach to the development of a nuclear magnetic resonance (NMR) gyro. Associated with the nuclei of Kr^{83} and Xe^{131}, and characteristic of nuclear spins greater than 1/2, is the nuclear quadrupole moment which interacts with electric field gradients. Field gradients arise at the nuclear site during collisions of noble gas atoms with the walls of their containers. This interaction is more pronounced in the Xe^{131} nuclear ensemble than in Kr^{83}. Attention is directed to the fact that, limited by this interaction, the transverse relaxation time (T_2) of the Xe^{131} nuclei published in available literature prior to this contract had been on the order of a few hundred milliseconds.* At the initial stage of this contract, it was improved to 5 to 10 seconds in 15 ml spherical samples. The extremely short T_2 made it difficult to improve our understanding on the subject of the alkali-atom-noble-gas-nucleus spin exchange interaction, which is essential for the development of an NMR gyro.

Both theoretical and experimental understanding of the nuclear quadrupole interaction continues to improve. In this section, we report T_2 of a Xe^{131} nuclear ensemble as long as 220 seconds. This improvement was accomplished by coating the cell wall with RbH. With the experimental advantage of a larger T_2, the parameters relevant to the nuclear quadrupole interaction were estimated for the first time. The results of investigations

---

*D. Brinkham, E. Brun, and H. H. Staub, Helv. Phys. Acta 35 431 (1962)

have been prepared as a scientific paper for consideration of
publication in the Physical Review. The preprint of this paper
is included in the Appendix to this section in lieu of a para-
phrased report on the research performed under this contract.
The developed process of data analysis can now be utilized
routinely in the gyro development to determine the characteris-
tics of cells containing Xe^{131} (or Kr^{83}) nuclei.

Investigations of noble gas nuclear quadrupole moments inter-
acting with the walls of their container will continue, particu-
larly for RbH coated glass walls. In order to improve the
uniformity of the coating, the reaction will be studied in glass
containers made of other than pyrex glass. Non-pyrex glass will
be studied because the rubidium reaction with hydrogen molecules
has been shown to be sensitive to the presence of impurities
(such as water, oxygen, etc.) normally embedded on pyrex glass.*

2.2 PUBLICATION PREPRINT

A copy of a preprint to be submitted to the Physical Review for
consideration of publication follows herein.

---

*A. Tam, G. Moe, and W. Happer, Phys. Rev. Lett. 35 1630 (1975)

Quadrupole nuclear spin relaxation of ^{131}Xe in the presence
of rubidium vapor

T. M. Kwon, J. G. Mark and C. H. Volk*

Litton Guidance & Control Systems

5500 Canoga Avenue, Woodland Hills, California, 91365

(Received

Nuclear spin relaxation of ^{131}Xe produced by collisions of
the xenon atoms with the walls of the experimental cell has been
studied. The xenon nuclear ensemble is polarized through spin
exchange collisions with an optically oriented rubidium vapor.
Depolarization of the ^{131}Xe ensemble in the wall collisions is
assumed to be due to the quadrupole coupling between the ^{131}Xe
nucleus and the electric field gradients which appear at the
nucleus during collisions of the atoms with the cell walls. Model
equations describing the nuclear relaxation are derived and
estimates of the electric field gradients are given.

I.   INTRODUCTION

We recently reported on measurements of the transverse nuclear spin relaxation of ^{83}Kr in the presence of rubidium vapor.[1] The decay of the krypton nuclear spin was found to be dependent on the orientation of the experimental cell with respect to an axis defined by the static magnetic field present in the apparatus. The angle between the cell and the magnetic field which yielded the longest decay time was termed the 'magic' angle after similar work done on ^{201}Hg[2]. Furthermore, we observed that the decay signal, off the magic angle, possessed a non-exponential character. These effects were modeled as an interaction between the nuclear quadrupole moment and the electric field gradients present at the krypton nucleus during collisions of the krypton atoms with the walls of the experimental cell. The model describes the transverse nuclear relaxation by 2I precessional frequencies, where I is the nuclear spin; I = 9/2, for ^{83}Kr. We are able to show a qualitative agreement between this model and the experimental measurements. A quantitative analysis of the krypton data was not possible due to the complexity of the signal.

We report here experimental data on the transverse nuclear spin decay of ^{131}Xe (nuclear spin, I = 3/2), which exhibits relaxation through an electric quadrupolar interaction in collisions with the cell walls. In order to simplify the experimental data analysis we have re-formulated our model of the nuclear quadrupolar interaction, viewing the precession of the nuclear ensemble as 2I oscillators each with a single frequency. In this way we treat 2I two-state Bloch type systems[3], instead of treating one complex system of 2I frequencies. This procedure is similar to the 'ficticious spin-1/2

operators' presented by Vega and Pines.[4] Furthermore, our previous model is extended in this work by incorporating results of a second order expansion of the nuclear density matrix as given by Cohen-Tannoudji for the case of relaxation of nuclear spin 3/2 under a quadrupolar interaction.[5] In this new model, we show that the second order expansion leads to a coupling among the 2I oscillators.

II. THEORETICAL MODEL

We consider in this section the transverse relaxation of a nuclear spin ensemble of nuclear spin I = 3/2 under a quadrupolar interaction. We will rely on results presented in Refs. (1 and 5) and repeat only selected details here, as clarity demands.

A. <u>The energy eigenvalues</u>. The full spin Hamiltonian of the system is taken to be:

$$H = H_M + H_Q \tag{1}$$

where H_M is the static magnetic interaction

$$H_M = - \hbar H_o I_z \tag{2}$$

with the nuclear gyromagnetic ratio, H_o the external magnetic field, taken to be along the z-axis, and I_z, the z-component of nuclear spin. H_Q, the quadrupolar Hamiltonian, represents the interaction of the nuclear electric quadrupole moment with an electric field gradient. As was argued in Ref. (1), the electric field gradient arises during collisions of the noble gas atoms with the walls of the experimental cell. If we assume that for a given collision, the resultant electric field

gradient possesses cylindrical symmetry, then the quadrupole Hamiltonian can be written as:[1,5,6]

$$H_Q = \frac{e^2 Qq}{4I(2I-1)} \left\{ \frac{1}{2} (3\cos^2\theta - 1) \left[3I_z^2 - I(I+1) \right] \right.$$

$$+ \frac{3}{2} \sin\theta \cos\theta \left[I_z(I^+ + I^-) + (I^+ + I^-)I_z \right] \tag{3}$$

$$\left. + \frac{3}{4} \sin^2\theta \, (I^{+2} + I^{-2}) \right\}$$

where e is the electronic charge, $eq = \partial^2 V/\partial z^2$, is the electric field gradient under the assumption of cylindrical symmetry, Q is the quadrupole moment of the noble gas nucleus, θ is the angle between the quantization axis and the cylindrical axis of the electric field gradient, and $I^\pm$ are the raising and lowering operators associated with the spin operator, I, where in the cartesian reference:[7]

$$I^\pm = I_x \pm iI_y \quad . \tag{4}$$

As in Ref. (1), we make the following definitions:

$$a = (3\cos^2\theta - 1), \tag{5a}$$

$$b = \sin\theta \cos\theta, \tag{5b}$$

$$c = \sin^2\theta, \tag{5c}$$

$$\alpha = e^2 Qq/4I(2I-1), \tag{5d}$$

and

$$\omega = -\gamma\hbar H_o. \tag{5e}$$

The quadrupole Hamiltonian, H_Q, is small compared to the magnetic Hamiltonian H_M, and thus we compute the energy eigenvalues for the full Hamiltonian employing perturbation theory[8]. The energy levels for a nucleus with spin 3/2 are computed through second order:

$$E_1 = \frac{3}{2}\omega + \frac{3}{2}\alpha a - \frac{27\alpha^2 b^2}{\omega} + \frac{27\alpha^2 c^2}{8\omega} \qquad (6a)$$

$$E_2 = \frac{1}{2}\omega - \frac{3}{2}\alpha a - \frac{27\alpha^2 b^2}{\omega} + \frac{27\alpha^2 c^2}{8\omega} \qquad (6b)$$

$$E_3 = -\frac{1}{2}\omega - \frac{3}{2}\alpha a + \frac{27\alpha^2 b^2}{\omega} - \frac{27\alpha^2 c^2}{8\omega} \qquad (6c)$$

$$E_4 = -\frac{3}{2}\omega + \frac{3}{2}\alpha a - \frac{27\alpha^2 b^2}{\omega} - \frac{27\alpha^2 c^2}{8\omega} \quad . \qquad (6d)$$

B. <u>The system equations</u>. The evolution of the observables of the system are found by solving the density matrix equation of the ensemble, which is given by:[9]

$$\frac{d\rho}{dt} = \frac{i}{\hbar} [\rho, H] \qquad (7)$$

and then computing the expectation value for a system observable, as:

$$<O> = Tr [\rho, O] \qquad (8)$$

where H is the Hamiltonian of the system given in Eq. (1), ρ is the density matrix of the nuclear ensemble and O is an operator corresponding to an observable of the system. For the situation represented by Eq. (1), in which there is a large time-independent interaction, H_M, and a much smaller but time-dependent term, $H_Q(t)$, it is convenient to transform the density matrix into the interaction representation, which is defined by:[10,11]

$$\rho(t) = e^{-(i/\hbar)H_M t} \rho^*(t) \, e^{(i/\hbar)H_M t} \qquad (9)$$

where $\rho^*(t)$ represents the density matrix in the interaction representation. The differential equation for ρ^* is easily found to be:

$$\frac{d\rho^*}{dt} = \frac{i}{\hbar} [\rho^*(t), H_Q^*(t)] \qquad (10)$$

where H_Q^* is given by:

$$H_Q^*(t) = e^{(i/\hbar)H_M t} H_Q(t) \, e^{-(i/\hbar)H_M t} \;. \qquad (11)$$

The time dependence of H_Q is taken to be that due to stochastic collisions of the xenon atoms with the walls of the experimental cell, in the same manner as that treated in Ref. (5).

In the limit that the quadrupole interaction can be taken as a perturbation, we solve Eq. (10) in an iterative manner[12], which through second order is given by:

$$\frac{d\rho^*}{dt} = \frac{i}{\hbar}\left[\rho^*(o), H_Q^*(t)\right]$$

$$+ \left(\frac{i}{\hbar}\right)^2 \int_o^t \left\{\left[\rho^*(o), H_Q^*(t')\right], H_Q^*(t)\right\} dt' \quad . \quad (12)$$

The first term in Eq. (12) was shown previously[1] to lead to a transverse decay of the nuclear ensemble through a dephasing of the precessing Zeeman levels. The second term in Eq. (12) has been treated by Cohen-Tannoudji[5] for the case of relaxation of ^{201}Hg under a quadrupole interaction. Since the nuclear spin of ^{201}Hg is 3/2, we can directly apply the results of Cohen-Tannoudji's work to our analysis of ^{131}Xe.

The commutators in Eq. (12) are evaluated under the following assumptions:

1. The first order commutator can be evaluated with a diagonal Hamiltonian whose eigenvalues are computed through second order; and,

2. The square of the product of the correlation time of the interaction, and the energy level separations of the nuclear Zeeman states, is much less than unity.

The first term in Eq. (12) is then evaluated by employing some straightforward matrix algebra, while the evaluation of the

second terms is found in Ref. (5). Eq. (12) is then written, transformed back into the Schroedinger representation, as:

$$[\dot{\rho}] = i \begin{bmatrix} 0 & -\Delta W_{12}\rho_{12} & -\Delta W_{13}\rho_{13} & -\Delta W_{14}\rho_{14} \\ \Delta W_{12}\rho_{21} & 0 & -\Delta W_{23}\rho_{23} & -\Delta W_{24}\rho_{24} \\ \Delta W_{13}\rho_{31} & \Delta W_{23}\rho_{32} & 0 & -\Delta W_{34}\rho_{34} \\ \Delta W_{14}\rho_{41} & \Delta W_{24}\rho_{42} & \Delta W_{34}\rho_{43} & 0 \end{bmatrix}$$

$$+ \frac{1}{T_Q} \begin{bmatrix} -2\rho_{11}+\rho_{22}+\rho_{33} & -3\rho_{12}+\rho_{34} & -3\rho_{13}-\rho_{24} & -2\rho_{14} \\ -3\rho_{21}+\rho_{43} & -2\rho_{22}+\rho_{11}+\rho_{44} & -2\rho_{23} & -3\rho_{24}-\rho_{13} \\ -3\rho_{31}-\rho_{42} & -2\rho_{32} & -2\rho_{33}+\rho_{11}+\rho_{44} & -3\rho_{34}+\rho_{12} \\ -2\rho_{41} & -3\rho_{42}-\rho_{31} & -3\rho_{43}+\rho_{21} & -2\rho_{44}+\rho_{22}+\rho_{33} \end{bmatrix}$$

(13)

where the first matrix in Eq. (13) is the result of the evaluation of the first order expansion in Eq. (12), with $\Delta W_{ij} = \overline{(E_i - E_j)}/\hbar$, where the bar represents a time average over the ij collision. The second matrix in Eq. (13) is taken from the results in Ref. (5), where from assumption 2 above, we have:

$$1/T_Q = J_o = J_1 = J_2 \quad . \tag{14}$$

The J_i's are the notation in Ref. (5) for the general decay rates due to a quadrupolar interaction. The condition in Eq. (14) results in a single exponential decay for the nuclear ensemble when the cell is oriented at the magic angle. This is observed experimentally.

The observable of interest in this particular experiment is the x-component of the noble-gas polarization[1,12], $<I_x>$. The corresponding operator for the spin 3/2 system, written in matrix form is:

$$I_x = (1/2) \begin{bmatrix} 0 & \sqrt{3} & 0 & 0 \\ \sqrt{3} & 0 & 2 & 0 \\ 0 & 2 & 0 & \sqrt{3} \\ 0 & 0 & \sqrt{3} & 0 \end{bmatrix} \quad . \tag{15}$$

The expectation value, $<I_x>$, is given by:

$$<I_x> = \mathrm{Tr}\left[I_x \rho\right] \quad . \tag{16}$$

For the spin 3/2 system, Eq. (16) becomes:

$$<I_x> = \frac{\sqrt{3}}{2}(\rho_{12}+\rho_{21}) + 2(\rho_{23}+\rho_{32}) + \frac{\sqrt{3}}{2}(\rho_{43}+\rho_{34}) \tag{17}$$

where the ρ_{ij}'s are the elements of the density matrix, with ρ_{ii} the population density of the state whose energy eigenvalue is given by E_i in Eq. (6). With the following definition:

$$M_{x1} = \frac{3}{2}(\rho_{12} + \rho_{21}) \tag{18a}$$

$$M_{x2} = (\rho_{23} + \rho_{32}) \tag{18b}$$

and,

$$M_{x3} = \frac{3}{2}(\rho_{34} + \rho_{43}) \tag{18c}$$

we can write Eq. (17) as:

$$\langle I_x \rangle = M_{x1} + M_{x2} + M_{x3} . \tag{19}$$

We have adopted the symbol 'M' for the sake of similarity to the Bloch equations[2]. The M's here represent a two-state polarization of the four state spin 3/2 system. In exactly the same manner, we can express the y-component of noble-gas polarization in terms of the two state polarizations, M_{y1}, M_{y2} and M_{y3}, appropriately defined. Using Eqs. (13 and 17-19) it is only a matter of algebra to show that the following set of equations describe the evolution of the nuclear ensemble under the quadrupolar interaction in terms of the two state polarizations:

$$
\begin{bmatrix}
\dot{M}_{x1} \\
\dot{M}_{y1} \\
\dot{M}_{x2} \\
\dot{M}_{y2} \\
\dot{M}_{x3} \\
\dot{M}_{y3}
\end{bmatrix}
=
\begin{bmatrix}
-3/T_Q & -\Delta W_{12} & 0 & 0 & 1/T_Q & 0 \\
\Delta W_{12} & -3/T_Q & 0 & 0 & 0 & 1/T_Q \\
0 & 0 & -2/T_Q & -\Delta W_{23} & 0 & 0 \\
0 & 0 & \Delta W_{23} & -2/T_Q & 0 & 0 \\
1/T_Q & 0 & 0 & 0 & -3/T_Q & -\Delta W_{34} \\
0 & 1/T_Q & 0 & 0 & \Delta W_{34} & -3/T_Q
\end{bmatrix}
\begin{bmatrix}
M_{x1} \\
M_{y1} \\
M_{x2} \\
M_{y2} \\
M_{x3} \\
M_{y3}
\end{bmatrix}
. \tag{20}
$$

Eq. (20) describes the evolution of a set of three oscillators. The coupling, which results from the inclusion of the second order terms, is between the first and third oscillators. If we neglect the coupling terms, the system equations are easily seen to reduce to the case treated in Ref. (1), with the solution given by Eq. (18) of Ref. (1). In addition, the uncoupled equations can each be written in the form:

$$M = (W \times M) + M/T_Q \tag{21}$$

which is exactly the form of the Bloch equations.[2]

Due to other relaxation effects on the ^{131}Xe ensemble, we have added an additional phenomenological term to all the diagonal elements. This procedure agrees with the results we have seen for the situation in which the quadrupole interaction is negligibly small.[13] The system of equations for the two-state polarizations then become:

$$
\begin{bmatrix}
\dot{M}_{x1} \\
\dot{M}_{y1} \\
\dot{M}_{x2} \\
\dot{M}_{y2} \\
\dot{M}_{x3} \\
\dot{M}_{y3}
\end{bmatrix}
=
\begin{bmatrix}
-\frac{3}{T_Q}-\frac{1}{T_2} & -\Delta W_{12} & 0 & 0 & \frac{1}{T_Q} & 0 \\
\Delta W_{12} & -\frac{3}{T_Q}-\frac{1}{T_2} & 0 & 0 & 0 & \frac{1}{T_Q} \\
0 & 0 & -\frac{2}{T_Q}-\frac{1}{T_2} & -\Delta W_{23} & 0 & 0 \\
0 & 0 & \Delta W_{23} & -\frac{2}{T_Q}-\frac{1}{T_2} & 0 & 0 \\
\frac{1}{T_Q} & 0 & 0 & 0 & -\frac{3}{T_Q}-\frac{1}{T_2} & -\Delta W_{34} \\
0 & \frac{1}{T_Q} & 0 & 0 & \Delta W_{34} & -\frac{3}{T_Q}-\frac{1}{T_2}
\end{bmatrix}
\begin{bmatrix}
M_{x1} \\
M_{y1} \\
M_{x2} \\
M_{y2} \\
M_{x3} \\
M_{y3}
\end{bmatrix}
\tag{22}
$$

where $1/T_2$ is the relaxation rate due to the other processes present in the cell, for instance, spin exchange of the ^{131}Xe nuclear spin with the rubidium valence electron.[13]

III. EXPERIMENT

The experimental apparatus and the generation of the signal from the noble gas nuclear ensemble has been previously discussed in detail.[14] We will describe here some of the salient features of the experimental set-up for the sake of the continuity of this report.

The experimental apparatus is shown schematically in Figure 1. The heart of the apparatus is the experimental cell, which is a 1-ml Pyrex sphere. The cell is sealed on a vacuum system with an excess of natural rubidium metal, 0.1 Torr enriched ^{129}Xe, 0.4 Torr enriched ^{131}Xe, 10 Torr N_2, 100 Torr He and 10 Torr H_2. Enriched ^{129}Xe consists of 61.22 mole % of ^{129}Xe and 13.44 mole % ^{131}Xe. Enriched ^{131}Xe contains 63.89 mole % ^{131}Xe and 0.7 mole % ^{129}Xe. Remaining components of each of the enriched species consist of even isotopes of xenon.[15] Since there is a ^{129}Xe impurity in enriched ^{131}Xe, enriched ^{129}Xe is added to the cell to ensure a sufficient ^{129}Xe signal so that the effects of the ^{129}Xe on the signal can be properly removed in the data analysis. The N_2 and the He are present to maximize the rubidium polarization, which is used to polarize the Xe noble gas ensembles through spin exchange.[14]

In order to simplify analysis of the experimental data in the light of the theory developed in Section II, the electric field gradient experienced by the ensemble of ^{131}Xe nuclei during collisions with the cell wall must be nearly cylindrically symmetric. It was found in the course of this work, that a cell

exhibiting field gradients of a cylindrically symmetric nature could be made by adding H_2 to the cell and baking the cell at 80°C for about two weeks.[16] During the baking period, the rubidium metal was held in the small region of the tip-off area of the spherical cell by forcing the tip region to be cool relative to the cell walls. Pyrex walls of the cells so processed were covered with milky particles, which we later identified as RbH.[17] Excess rubidium metal was still present in the cell. When the cell wall was coated uniformly with RbH, the imaginary axis diametrically through the tip of the cell was found to correspond to the axis of cylindrical symmetry of the quadrupolar interaction. This condition was verified experimentally if a cell showed the magic angle behavior when the angle between the magnetic field and the imaginary axis through the tip was approximately 55°. No such symmetry could be observed in the cells for which no processing was done. It was further noted that [131]Xe polarization is much higher in the RbH coated cells than in the cells without coating.

Within the experimental apparatus the cell is centered in a resistance-heated oven, provided with Pyrex windows at either end. The oven controls the temperature to within ±0.1°C with a temperature uniformity across the cell of about 0.5°C. The cell is mounted in a holder which allows it to be rotated in two dimensions from outside the apparatus with a precision of 0.5 deg. The oven is contained in a cylindrical coil form, providing three mutually perpendicular Helmholtz coils. The oven assembly is within four cylindrically concentric magnetic shields. These shields reduce the external magnetic fields to below 10 μG.

The instantaneous transverse polarization of the noble gas ensembles are determined by measuring the effective magnetic fields of these polarized ensembles. The nuclear ensembles are

polarized in spin exchange collisions with the optically oriented
rubidium vapor. The rubidium vapor is optically pumped by
illuminating the cell with D_1 circularly polarized light from a
rubidium discharge lamp. Detection of the effective magnetic
fields generated by the polarized nuclear ensembles is accom-
plished by utilizing the rubidium vapor as a magnetometer. This
technique has been thoroughly discussed in the literature[18,19]
and our particular mechanization has been previously described.[14]
The axes for this work have been labelled in a slightly different
manner than what was done in Ref. (14). This change was made to
facilitate the form of the model equations and presents no
difficulty in applying the results as displayed in Ref. (14) to
this work.

The particular experimental procedures for this work are as
follows. In the presence of the light, a 2 mG field is applied
initially along the y-axis, as defined in Figure 1. This condi-
tion continues for 10 min., in which time a significant noble
gas nuclear polarization is built up. The y-field is then
switched to zero while a precessional magnetic field of 350 μG
is applied along the z-axis together with an ac magnetic field
(H_{ac}) along the x-axis, which defines the sensitive axis of the
rubidium magnetometer. The cell is arranged in the apparatus
with the cell's imaginary axis in the x-z plane. The imaginary
axis of the cell can be rotated a full 360 degrees in this plane.
As we noted earlier, the imaginary axis diametrically through
the tip of the cell has been found to be the cylindrically
symmetric axis of the quadrupole interaction. Rotation of the
imaginary axis in the x-z plane then corresponds to a rotation
of the cell through the angle as defined in Eq. (3). There is
an additional ability to rotate the cell's imaginary axis ±5
degrees out of the x-z plane. This feature was employed to check
the assumption of cylindrical symmetry of the interaction. The

geometry of the cell is shown in Figure 2. 4000 data points at
equal time intervals over 300 seconds are taken after the
y-magnetic field is switched off. Angle data at 10 deg. cell
angle increments in the x-z plane was taken. The data from
the first half cycle, 0 to 180 deg. is presented in this report.
All data in this report were acquired at a cell temperature of
81.3°C ±0.5°C.

IV. ANALYSIS

A. The signal form. In order to facilitate the data reduction,
we re-write the form of the two-state polarization equations
from that given in Section II. For brevity, we introduce the
following notation:

$$\omega_c = \omega + \frac{54 b^2 \bar{\alpha}^2}{\omega} \tag{23a}$$

$$\omega_1 = \Delta W_{12} = \omega_c + 3\bar{\alpha}a \tag{23b}$$

$$\omega_2 = \Delta W_{23} \tag{23c}$$

$$\omega_3 = \Delta W_{34} = \omega_c - 3\bar{\alpha}a \tag{23d}$$

where $\bar{\alpha}$ represents a time average of α over the collisions.
Eq. (22) can be conveniently broken in two parts, due to the
particular coupling among the oscillators. One equation to
represent the second oscillator, subscripted '2', with frequency
ω_2 and a set of equations for oscillators '1' and '3', with
frequencies ω_1 and ω_3, respectively. We take advantage of the
symmetric separation in these two oscillator frequencies from

the center frequency, ω_c, and write M_x for oscillator 1 and 3 as:

$$M_{xs} = M_{xs}^O e^{-(p+r)t} F(\theta) \sin(\omega_c t) \tag{24}$$

$$F(\theta) = \begin{cases} \cosh(\varepsilon t) + (r/\varepsilon) \sinh(\varepsilon t) & r>3\bar{\alpha}a \\ 1 + rt & r=3\bar{\alpha}a \\ \cos(\varepsilon t) + (r/\varepsilon) \sin(\varepsilon t) & r<3\bar{\alpha}a \end{cases} \tag{25a}$$

$$p = \frac{1}{T_2} + \frac{2}{T_Q} \tag{25b}$$

$$r = \frac{1}{T_Q} \tag{25c}$$

$$\varepsilon^2 = |r^2 - (3\bar{\alpha}a)^2| \tag{25d}$$

where the subscript 's' denotes either 1 or 3 and M_{xs}^O is the initial amplitude of the signal for these oscillators. The frequency of the second oscillator, ω_2, can be written as:

$$\omega_2 = \omega_c + \Delta\omega_2 \tag{26}$$

where

$$\Delta\omega_2 = -\frac{108\bar{\alpha}^2 b^2}{\omega} + \frac{27\bar{\alpha}^2 c^2}{4\omega} \quad . \tag{27}$$

$\Delta\omega_2$ is due to a second order effect, which is negligibly small. In this limit we can write the expression for the second oscillator as:

$$M_{x2} = M_{xc}^O e^{-pt} \sin(\omega_c t) \quad . \tag{28}$$

If we assume that the initial amplitudes of the first and third oscillators are equal, we can then write the expression for the signal as given in Eq. (19) as:

$$M_x = M_{xc}^O e^{-pt} [1 + Me^{-rt} F(\theta)] \sin(\omega_c t) \tag{29}$$

where the ratio of the oscillator amplitudes, M, is given by:

$$M = 2M_{xs}^O / M_{xc}^O \quad . \tag{30}$$

At the magic angle, i.e., where a = 0, Eq. (29) is seen to reduce to:

$$M_x = M_{xc}^O [1 + M] e^{-pt} \sin(\omega_c t) \quad . \tag{31}$$

Eq. (31) is seen to represent a single exponentially decaying sinusoid, which is what is experimentally observed.[1]

B. _Data reduction_. As we previously stated, ^{131}Xe is not commercially available without a ^{129}Xe impurity. For this reason, we chose to enhance the unwanted ^{129}Xe signal by adding enriched ^{129}Xe to the cell so that we could ensure its complete

removal from the data before we analyzed the decay of the ^{131}Xe ensemble.

Typical raw data is displayed in Figure 3. This data was taken off the magic angle, thus the non-exponential character of the ^{131}Xe decay is clearly observed. Since the nuclear spin of ^{129}Xe is 1/2, its decay at all cell orientations is simple exponential. The form of the ^{129}Xe decay is thus exactly known and we then utilized a Kalman filtering technique to remove this signal from the raw data. The Kalman technique was used since this method was designed to remove 'signals' buried in noise. In this situation, we simply treat the ^{131}Xe signal and the noise as 'noise' and remove a single exponentially decaying sinusoid representing the effects of ^{129}Xe. The result of this processing is displayed in Figure 4. A 'fast fourier transform' was then performed on the data with the ^{129}Xe signal removed to verify that the ^{129}Xe had been completely removed.

Due to the subtle differences between data fitting with a Kalman technique and a Least Squares method[22], we chose to employ a Least Squares routine to fit the ^{131}Xe data to our model. We used an eight parameter fitting routine of the form:

$$S = x_3 e^{-(x_4 + 2x_5)t} [1 + M e^{-x_5 t} F(\theta)] \sin (x_1 + x_2 t) + x_7 + x_8 t \quad (32)$$

$$F(\theta) = \begin{cases} \cos(x_6 t) + (x_5/x_6) \sin (x_6 t) & (33a) \\ \cosh (x_6 t) + (x_5/x_6) \sinh (x_6 t) \ . & (33b) \end{cases}$$

Eq. (32) was used with Eq.'s (33a) and (33b) for the angle data far from the magic angle and very near the magic angle,

respectively. In Eq.'s (32 through 33b), the eight parameters
represent the following terms:

$$x_1 = \text{initial phases} \qquad (34a)$$

$$x_2 = \omega_c \qquad (34b)$$

$$x_3 = M_{xc}^O \qquad (34c)$$

$$x_4 = 1/T_2 \qquad (34d)$$

$$x_5 = 1/T_Q \qquad (34e)$$

$$x_6 = \left| \left(\frac{1}{T_Q}\right)^2 - \left[\left(\frac{\tau_s}{\tau_s+\tau_v}\right) \frac{e^2 Qq}{4} \left(3 \cos^2\theta - 1\right) \right]^2 \right|^{\frac{1}{2}} \qquad (34f)$$

$$x_7 = \text{dc offset of the signal} \qquad (34g)$$

$$x_8 = \text{linear drift in the dc offset.} \qquad (34h)$$

The factor $\tau_s/(\tau_s+\tau_v)$ in Eq. (34f) results from the time
average of the dephasing terms over the duration of the collision.
τ_s is the duration of the interaction, that is the sticking time
on the wall, and τ_v is the time between collision.

In the fitting routine, we have set the initial phases of
the three oscillators to be equal. There is no a priori reason
why this should not be and we observe nothing in the results of
our data fit to indicate that this is not a valid assumption.

We further had to make an assumption concerning the ratio of the oscillator amplitudes, M given by Eq. (30). An attempt to let this vary in the Least Squares routine resulted in instabilities in the data fit. In Ref. (1), we considered the case of low polarization.[23] In this limit, using Eq. (8 and 10) of Ref. (1) and Eqs. (18a-c) we find:

$$M^O_{x1} : M^O_{x2} : M^O_{x3} = 3 : 4 : 3 \quad . \tag{35}$$

In the limit of complete polarization, on the other hand, which implies $\rho_{11}=1$ in Eq. (8) of Ref. (1), we find:

$$M^O_{x1} : M^O_{x2} : M^O_{x3} = 1 : 2 : 1 \quad . \tag{36}$$

We have good reason to believe that for these experiments, the nuclear ensemble was not in the low polarization limit, however, we also definitely know that the nuclear ensemble did not attain 100% polarization, this implied:

$$1 < M < 1.5 \tag{37}$$

where 1 is the limit of complete polarization and 1.5 is the low polarization limit. We additionally demand that this ratio remain constant over all the angles at a given temperature and pumping time. This is, as was argued in Ref. (1), due to the fact that the first order quadrupolar interaction does not enter into the longitudinal relaxation of the noble gas ensemble and hence cannot affect the initial amplitude of the signal. By employing different ratios under the above constraints in the eight parameter fitting routine, we found that M = 1.35 gave the best results. This value was then fixed in the routine.

V. RESULTS

The three parameters of interest in the eight parameter Least Squares routine are x_4, x_5 and x_6. From these terms we derive the phenomenological relaxation rate,

$$\frac{1}{T_2} = (3.76 \pm .41) \times 10^{-3} \text{ sec}^{-1} \qquad (38)$$

and the transverse quadrupole relaxation rate,

$$\frac{1}{T_Q} = (5.94 \pm .65) \times 10^{-4} \text{ sec}^{-1} \ . \qquad (39)$$

The angularly dependent dephasing rate, $3\bar{a}a$, is displayed in Figure 5. The errors associated with the derived terms represent one standard deviation. The solid line in Figure 5 represents a Least Squares fit of the time average of the dephasing rate to the equation:

$$A(\theta) = \left(\frac{\tau_s}{\tau_s + \tau_v}\right) \frac{e^2 Qq}{4} [3 \cos^2 \theta - 1] \ . \qquad (40)$$

where θ is the angle between the magnetic field axis (z-axis) and the imaginary axis diametrically through the tip of the cell. From the fit we find:

$$A(\theta) = (8.9 \pm 0.4) \times 10^{-3} [3 \cos^2 \theta - 1] \ . \qquad (41)$$

Comparing Eq. (40) and Eq. (41) we find:

$$\left(\frac{\tau_s}{\tau_s + \tau_v}\right) e^2 Qq = 3.56 \times 10^{-2} \text{ sec}^{-1} \ . \qquad (42)$$

We can estimate the sticking time on the wall, τ_s, by assuming a simple adsorption model. The sticking time is then given by[24]:

$$\tau_s = \tau_o e^{E_a/kT} \tag{43}$$

where τ_o is taken to be 10^{-12} sec, and E_a is the adsorption energy. Taking E_a to be 0.13 eV[13], we compute: $\tau_s = 6.6 \times 10^{-11}$ sec. τ_v is the time between wall collisions, and it can be estimated from simple gas kinetic arguments:[25]

$$\tau_v = 4 \text{ Vol}/vA_s \tag{44}$$

where Vol is the volume of the cell, A_s is the surface area and v is the kinetic velocity of the xenon atoms. Evaluating Eq. (44) for our experimental conditions yields: $\tau_v = 3.5 \times 10^{-5}$ sec. Since $\tau_s << \tau_v$, we can neglect τ_s in the denominator of Eq. (42) and calculate the average electric field gradient:

$$eq = -3.45 \times 10^{11} \text{ statcoulombs cm}^{-3} . \tag{45}$$

Recently Keenan et al[26] estimated the electric field gradient which arises at the nucleus of a ^{131}Xe atom due to a distortion of the spherical shells. This distortion takes the form of electronic excitation with dipole selection rules. They assumed a one electron model and the excitation $5p^6 \to 5p^5 6s$. The field gradient was then estimated to be:

$$eq = -7.0 \times 10^{12} \text{ statcoulombs cm}^{-3} . \tag{46}$$

Given the approximations, we find our value in good agreement with this estimate.

The transverse quadrupole rate is given in Ref. (5) as:

$$\frac{1}{T_Q} = \frac{36\Pi}{5} \frac{\tau s}{\tau_s + \tau_v} \left[\frac{e^2 Q q}{3}\right]^2 \tau_c \quad .\tag{47}$$

From our measured value of the quadrupole relaxation rate given in Eq. (39), and our estimate of the electric field gradient strength given in Eq. (45), we compute the correlation time for this interaction to be: $\tau_c = 3.5 \times 10^{-7}$ sec.

Finally as a check on our parameter fit, we compare the phenomenological relaxation rate of the ^{131}Xe with the decay rate of the ^{129}Xe signal. From previous measurements[13,14] on the decay of ^{129}Xe and ^{131}Xe, we predict that at this temperature the predominant relaxation is due to spin exchange collision of the xenon atoms with the rubidium vapor. We then write:

$$\frac{1}{T_2} = N_{Rb} \, \sigma_{ex} \, V_{rel}\tag{48}$$

where N_{Rb} is the rubidium density, σ_{ex} is the Rb-Xe spin exchange cross section and V_{rel} is the relative Rb-Xe velocity. The ratio of relaxation rates is simply the ratio of cross section for spin exchange. From the ^{129}Xe signal, which we extracted from the original data, we found:

$$1/T = \left(1.34 \pm 0.7\right) \times 10^{-2} \text{ sec}^{-1}\tag{49}$$

and thus we estimate the cross section ratio to be:

$$\sigma_{ex}^{129} / \sigma_{ex}^{131} = 1/3.56 \quad .\tag{50}$$

From Herman's model of Rb-noble-gas spin exchange we predict the ratio of cross sections to be[27]:

$$\sigma_{ex}^{129} / \sigma_{ex}^{131} = 1/2.28 \quad . \tag{51}$$

We believe that this is very good agreement supporting the validity of our fitting procedure, and that the difference between Herman's prediction and our estimate is due to the contribution of the Rb-Xe van der Waals molecules in the alkali-noble-gas spin exchange interaction.[14,28]

VI. DISCUSSION

We have investigated the nuclear transverse spin relaxation of ^{131}Xe under a quadrupole coupling between the ^{131}Xe nucleus and the electric field gradients which arise at the nucleus during collisions of the xenon atoms with the walls of the cell. We picture the collisions as resulting in a deformation of the xenon electronic shells. It is this deformation which produces the electric fields at the xenon nucleus. The angular dependence of this interaction is interpreted to mean that adsorption sites on the cell walls have a non-isotropic distribution. Further supporting this view is our finding of a dependence of this interaction on the distribution of the metalic rubidium on the cell walls. A nearly uniform distribution of the rubidium reservoir over the surface of the cell results in a very strong relaxation of the ^{131}Xe ensemble, in fact complete relaxation is found to take place in a few precessional periods, and thus usable data cannot be obtained. In the cells that are uniformly coated with RbH, the adsorption sites on the walls appear to be isotropic with the location of excess rubidium metal being different from the rest. Relaxation data that fit to our model

are obtained only in those RbH-coated cells in which the rubidium metal is driven to the tip of the cell.

We believe that our technique of observing this effect is quite valuable since we obtain information from both the dephasing and transverse relaxation, which have different dependencies on the interaction parameters. We have, however, still not been able to definitely determine the adsorption energy or sticking time of the xenon atoms on the cell wall or the correlation time of the interaction, and thus a precise value of the electric field gradient, which we estimated, remains in some question. We have begun experiments to investigate these two parameters which will allow us to make a better determination of the interaction strength.

ACKNOWLEDGEMENTS

REFERENCES

*Present address: The Aerospace Corp., P.O. Box 92957, Los Angeles, California, 90009.

1. C. H. Volk, J. G. Mark and B. C. Grover, Phys. Rev. A $\underline{20}$, 2381 (1979).

2. D. S. Bayles, I. A. Greenwood and J. H. Simpson, "Noise Sources in NMR Oscillaotrs and Relaxation Phenomena in Optically Pumped Mercury Isotopes", Final Scientific Report, AFOSR, 1976 (unpublished).

3. F. Bloch, W. W. Hansen, and M. Packard, Phys. Rev. $\underline{69}$, 127 (1946); Phys. Rev. $\underline{70}$, 474 (1946).

4. S. Vega and A. Pines, J. Chem. Phys. $\underline{66}$, 5624 (1977).

5. C. Cohen-Tannoudji, J. Phys. (Paris) $\underline{24}$, 653 (1963).

6. I.. Abragam, The Principles of Nuclear Magnetism, (Clarendon, Oxford, 1961) Chap. 8.

7. L. I. Schiff, Quantum Mechanics, (McGraw-Hill, New York, 1968), p. 200.

8. L. I. Schiff, in Ref. 7, p. 247.

9. U. Fano, Rev. Mod. Phys. $\underline{29}$, 74 (1957).

10. A. Messiah, Quantum Mechanics, (John Wiley & Sons, New York, 1958), pp. 314-317.

11. C. P. Slichter, Principles of Magnetic Resonance, (Springer-Verlag, New York, 1978), p. 157.

12. C. P. Slichter, in Ref. 11, p. 158.

13. C. H. Volk, T. M. Kwon, J. G. Mark, Y. B. Kim, and J. C. Woo, Phys. Rev. Lett. $\underline{44}$, 136 (1980).

14. C. H. Volk, T. M. Kwon, and J. G. Mark, Phys. Rev. A 21, 1549 (1980).

15. Purchased from Monsanto Research Corp., Miamisburg, Ohio 45342.

16. One of us (TMK) has disclosed a patent on this technique.

17. A. Tam, G. Moe and W. Happer, Phys. Rev. Lett. 35, 1630 (1975).

18. C. Cohen-Tannoudji, J. Dupont-Roc, S. Haroch, and F. Laloe, Rev. Phys. Appl. 5, 102 (1970).

19. C. Cohen-Tannoudji, J. Dupont-Roc, S. Haroch, and F. Laloe, Phys. Rev. Lett. 22, 758 (1969).

20. R. E. Kalman, Trans. ASME, J. Basic Eng., 82D, 34 (1960).

21. R. E. Kalman and R. Bucy, Trans. ASME, J. Basic Eng., 83D, 95 (1961).

22. A Kalman filter yields the best estimate of the parameter set at a given point based on all past measurements, whereas a Least Squares technique gives the best global estimate of the parameter set based on all measurements. In the limit that the model is exact the Kalman filter and the Least Squares method are identical. In our situation, the form of the ^{129}Xe signal is known exactly, thus it is expedient to remove its effects with the Kalman filter. Due to the estimates used in arriving at the form of the ^{131}Xe signal, we chose to use the Least Squares technique and estimate the parameters on the global sense of the data.

23. L. W. Anderson and A. T. Ramsey, Phys. Rev. 124, 1862 (1961).

24. J. H. Deboer, The Dynamical Character of Adsorption, (Oxford, U. P., New York, 1963).

404577

25. E. H. Kennard, <u>Kinetic Theory of Gases</u>, (McGraw-Hill, New York, 1938), p. 63.

26. M. R. Keenan, L. W. Buxton, E. J. Campbell, T. J. Balle, and W. H. Flygare, J. Chem. Phys. <u>73</u>, 3523 (1980).

27. R. M. Herman, Phys. Rev. <u>137</u>, A1062 (1965).

28. N. D. Bhaskar, M. Hou, M. Ligare, B. Suleman, and W. Happer, Phys. Rev. A <u>22</u>, 2710 (1980).

FIGURE CAPTIONS

Figure 1.   Schematic representation of the experimental
            apparatus

Figure 2.   Geometrical arrangements of the experimental cell

Figure 3.   Typical example of the raw signal. Low frequency
            component is due to the ^{131}Xe precession, while the
            high frequency is the ^{129}Xe signal. This data was
            taken at the cell orientation at which the magnetic
            field axis coincides with the imaginary axis
            diametrically through the tip of the spherical cell.

Figure 4.   Typical example of the signal after the effects of
            the ^{129}Xe have been removed. The data shown in
            Figure 2-3 are displayed.

Figure 5.   Quadrupole dephasing terms as a function of angle.
            The error bars on the data points represent one
            standard deviation and the solid line is a Least
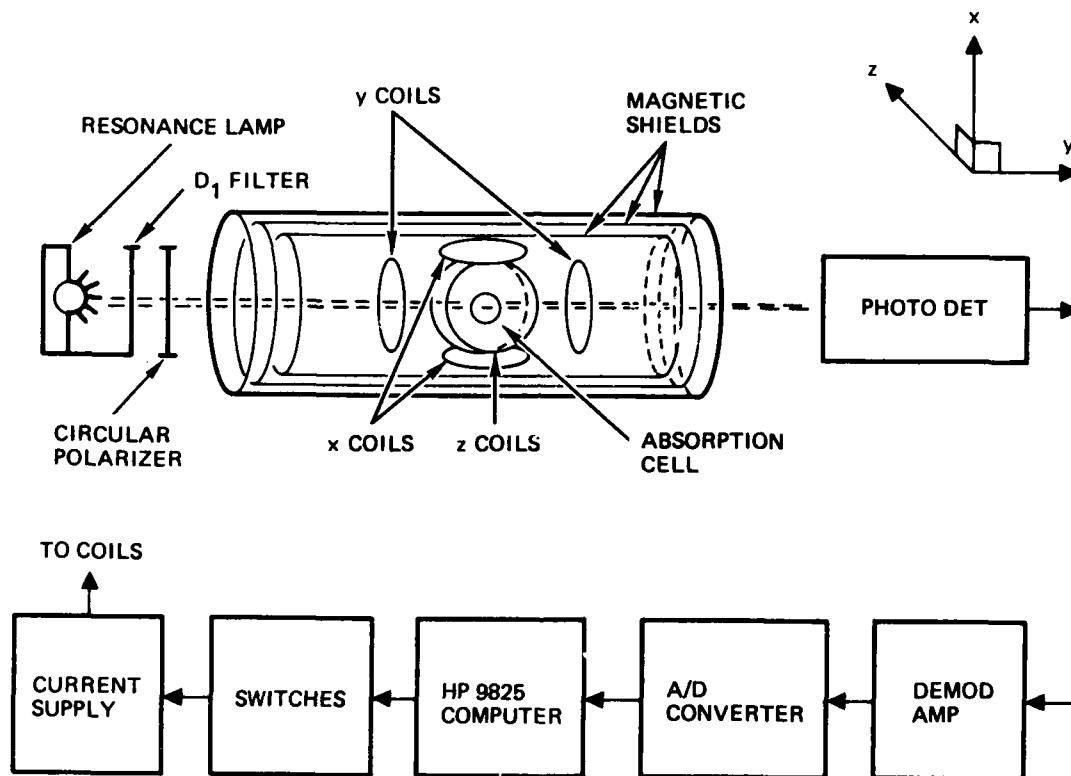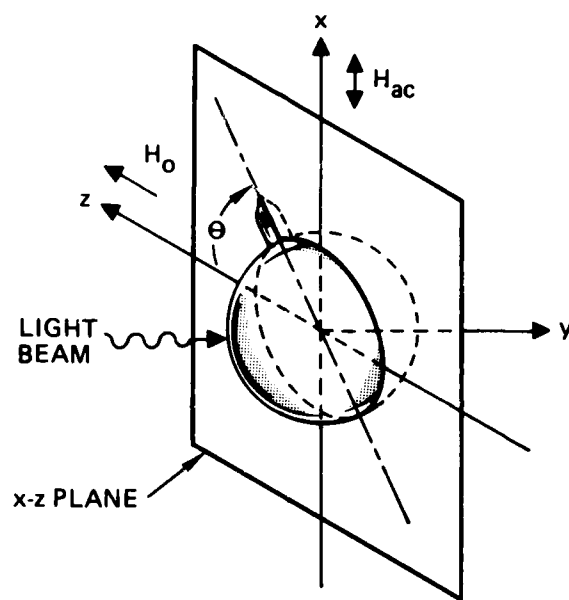   Squares fit to the data.

Figure 1
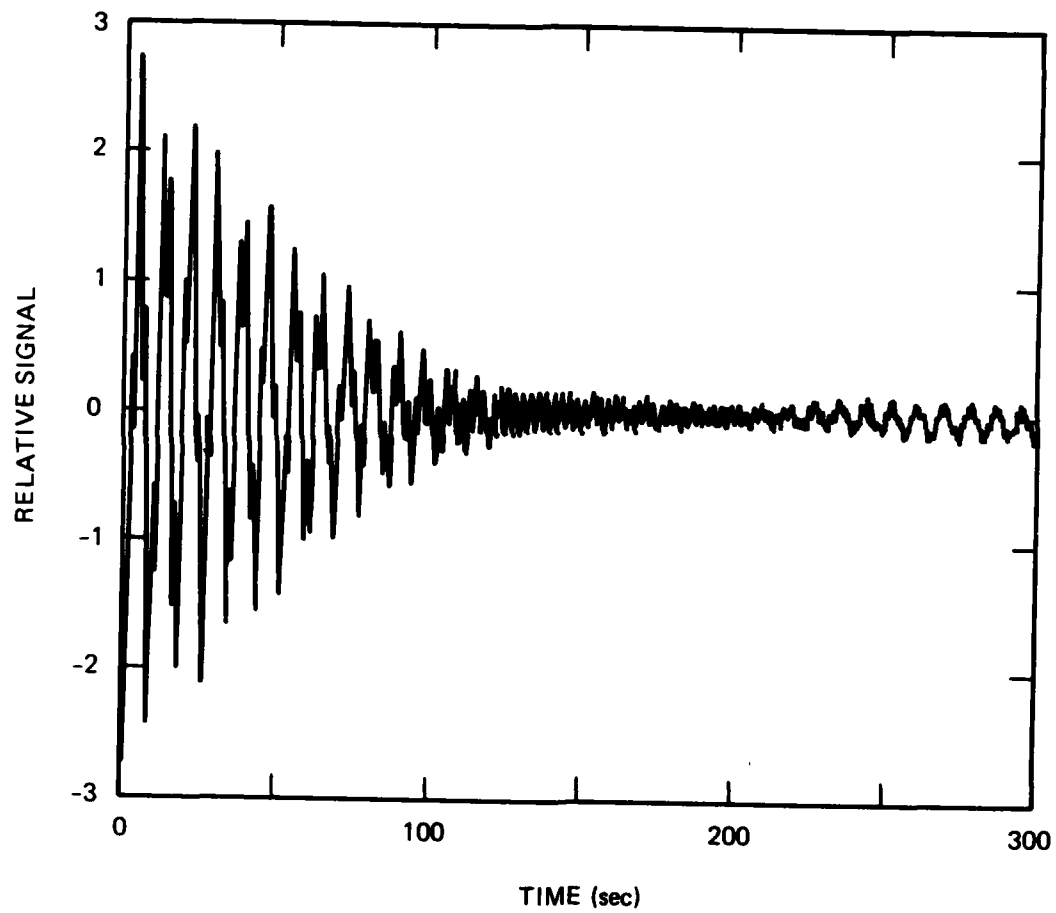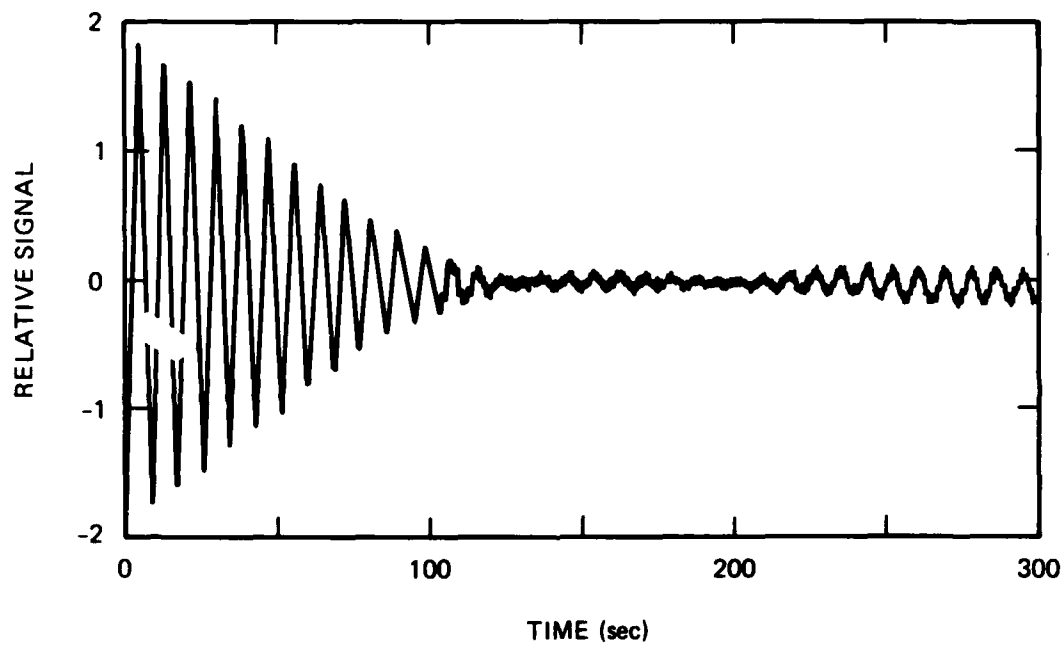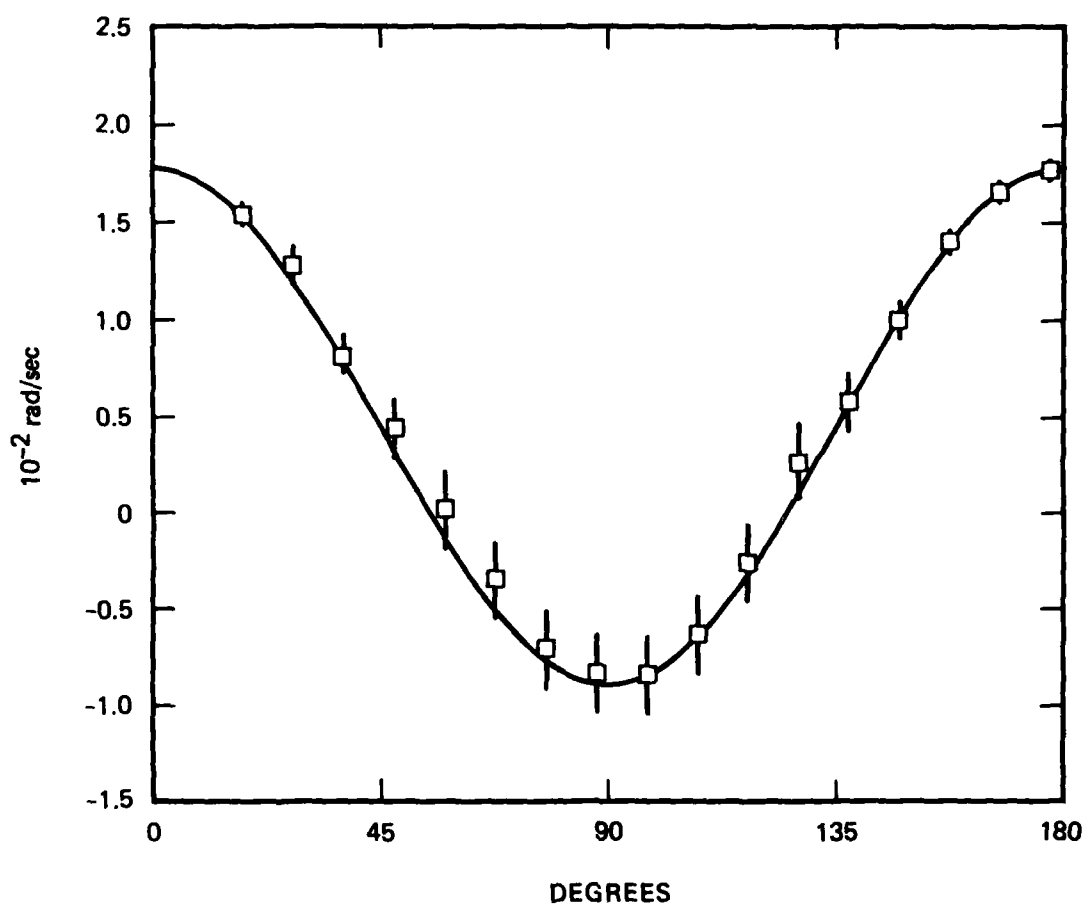
Figure 2

Figure 3

Figure 4

Figure 5

SECTION III

NOBLE GAS NUCLEAR FREQUENCY SHIFT

3.1   INTRODUCTION

The shift of the precessional frequency of the noble gas nucleus
in a magnetic field reported in this section is associated with
the transfer of angular momentum from an electronically polarized
alkali atom to an unpolarized noble gas nucleus in the spin
exchange process. Such frequency shift has been reported for the
case of free electrons interacting with optically pumped alkali
atoms[1-3]. No such information is yet available to our knowledge
for noble gas nuclei, such as Kr^{83}, Xe^{129} and Xe^{131}.

Since the angular rate in the nuclear magnetic resonance (NMR)
gyro is sensed as a shift in the precession frequency of certain
nuclear species, the information regarding the frequency shift
can lead to a determination of gyro bias shift due to the spin
exchange interaction with the polarized alkali-vapor. As will be
shown later, the frequency shift of the noble gas nucleus is
strongly dependent on <u>both</u> the number density of the alkali-atom
and the alkali polarization. This would mean that the same
information would also lead to determinations of temperature
dependence and the alkali-pumping light intensity dependence of
the NMR gyro bias.

In this section we review briefly the theoretical background of
the spin exchange interaction to give an understanding of the
frequency shift, and subsequently present the experimental
results.

3.2 THEORY OF FREQUENCY SHIFT

In order to review the theory, we will rely on the results previously reported[4], and repeat only selected details here as clarity demands.

We start with Herman's effective interaction Hamiltonian between an alkali atom and noble gas nucleus in the form[5]:

$$\mathcal{H}_{eff} = (\frac{16\pi}{3}) \, g_N \mu_N \mu_o \mu_1 (B)^2 \eta^2 \vec{I} \cdot \vec{S} \qquad (52)$$

where $\vec{I}$ is the noble-gas nuclear spin, $\vec{S}$ the alkali electronic spin, g_N the nuclear g-factor, μ_N the nuclear magneton, and μ_o the Bohr magneton. η is the exchange enhancement factor, given by.

$$\eta(R) = \left[1 - \sum_{i=2}^{n} \frac{<i|1> \, u_i(B)}{u_1(B)} \right] \qquad (53)$$

where R is the internuclear separation between the alkali and noble gas atoms. The summation over i refers to the alkali valence electron (1) and the noble gas electrons (2,3...,n). The factors $<i|1>$ are the overlap integrals and $u_i(B)$ is the amplitude of the ith orbital of the isolated atom at the noble gas nucleus, B. For the internuclear separation of $R = 7.8a_o$ (a_o is the unit of atomic distance; $a_o = 0.529 \times 10^{-8}$ cm), the values of η for the Rb-Kr and Rb-Xe system have been calculated to be[4]:

$$\eta_{Kr} = 40 \quad \text{and} \quad \eta_{Xe} = -59 \ . \qquad (54)$$

We consider a gaseous mixture of alkali and noble gas atoms
subjected from the outside only to a constant uniform magnetic
field, but interacting with each other through the relatively
short range forces, so that the otherwise free atoms occasionally
collide with each other. These collisions may be either of the
binary type or molecular forming (three body) type. All colli-
sions are such that the mean time between collisions, τ_A, is long
compared to the duration of the collision, τ_D. It is further
assumed that the external magnetic field is so weak that the pre-
cession frequencies of the electron moment and the nuclear moment
are orders of magnitude smaller than the strength of the inter-
action given by Eq. (52), when the internuclear separation is
within the atomic range.

In what follows we take the total Hamiltonian acting on the spin
variables to be:

$$\mathcal{H} = -\hbar\omega_S S_z - \hbar\omega_I I_z + [\hbar\gamma(R)\,\vec{I}\cdot\vec{S}\,] \tag{55}$$

where the first two terms of the right hand side of the equation
are the coupling to the external magnetic field, which will be
represented by $\mathcal{H}_o$, and the last term represents the exchange
interaction, where $\gamma(R)$ is the strength of the interaction:

$$\gamma(R) = \left(\frac{16\pi}{3}\right) g_N\mu_N\mu_o u_1(B)^2\,\eta(R)^2/\hbar \ . \tag{56}$$

$\gamma(R)$ falls off rapidly with internuclear separation, R, and thus
the kinematics of the interaction is to picture the spins before
a collision as acted on by $\mathcal{H}_o$, then coming under the combined
action of $\mathcal{H}_o + \hbar\gamma(R)\vec{I}\cdot\vec{S}$ during the interaction and finally, as the
particles separate, going back to the uniform precession of $\mathcal{H}_o$.

We now consider a much simplified system consisting of an atom with a single electron in a $2S_{1/2}$ state and no nuclear spin (the alkali atom $\vec{S}=1/2$) and an atom with no electronic spin, $\vec{S}=0$ and nuclear spin $\vec{I}=1/2$ (the noble gas atom). The system is described quantum mechanically by a density matrix of $(2S + 1)(2I + 1)$ dimensions, namely, by a 4 x 4 matrix.

The density matrix can be constructed in the representation of the ortho-normal set of eigenfunctions of I^2, I_z, and S^2, S_z for the free (noninteracting) atoms. The time development of the density matrix resulting solely from the spin exchange interaction can then be investigated in the interaction representation.

The derivation of the shift of the noble gas nuclear precession frequency involves the equation of motion for the mean value of the operator I^+ (or I^-), where, as commonly defined, $I^{\pm} = I_x \pm i\, I_y$, in the Schrödinger representation. Following the work of Major[6], it has been shown that

$$\frac{d}{dt} <I^+> = -\frac{1}{\tau_A}\left[\frac{(1/2)\gamma_{ave}^2 \tau_D^2}{1+\gamma_{ave}^2 \tau_D^2} - i <S_z> \frac{\gamma_{ave}\tau_D}{1+\gamma_{ave}^2 \tau_D^2}\right] <I^+> \qquad (57)$$

$$-\frac{1}{T_2} <I^+>$$

where γ_{ave} is the strength of the spin exchange interaction, given by Eq. (56), averaged over the collisional parameters.

The real part of the coefficient of $\langle I^+ \rangle$ represents the phase coherence decay time, T_{ex}, due to the spin-exchange interaction, i.e.,

$$T_{ex}^{-1} = \frac{1}{2}\left(\frac{1}{\tau_A}\right)\frac{\gamma_{ave}^2 \tau_D^2}{1 + \gamma_{ave}^2 \tau_D^2} \quad . \tag{58}$$

The imaginary term, which is <u>seen</u> to be proportional to the electron spin polarization, represents a shift in the precession frequency of the nuclear spin in the external magnetic field:

$$\Delta\omega = \left(\frac{1}{\tau_A}\right)\frac{\gamma_{ave}\tau_D}{1 + \gamma_{ave}^2 \tau_D^2} \langle S_z \rangle \quad . \tag{59}$$

This shift can be written as an equivalent magnetic field, given by:

$$\Delta H = \left(\frac{1}{g_N \mu_N}\right)\left(\frac{1}{\tau_A}\right)\frac{\gamma_{ave}\tau_D}{1 + \gamma_{ave}^2 \tau_D^2} \langle S_z \rangle \tag{60}$$

where ΔH is now a magnetic field 'experienced' by the noble gas atoms due to the presence of the alkali atom.

3.2.1 Frequency Shift Due to Exchange Process of the Binary Type

Consider the spin exchange process due to the binary type collisions, for which $\gamma_{ave}\tau_D \ll 1$[7]. Eq. (60) can now be written as:

$$\Delta H \approx \left(\frac{1}{g_N \mu_N}\right)\left(\frac{1}{\tau_A}\right)\gamma_{ave}\tau_D \langle S_z \rangle \quad . \tag{61}$$

The collision rate can be written as:

$$\tau_D = \pi \overline{d}^2 \, N_A \, v_{rel} \qquad (62)$$

where $\overline{d}$ is the mean interaction distance and N_A is the alkali atom number density. v_{rel} is the mean relative velocity between the alkali atoms and noble-gas atoms. The binary collision duration is taken to be:

$$\tau_D = \frac{\overline{d}}{v_{rel}} \; . \qquad (63)$$

Combining Eq's. (62) and (63) with the definition of γ given in Eq. (56), Eq. (61) is found to be:

$$\Delta H = \frac{16\pi^2}{3} \, \overline{d}^3 \, N_A \mu_o \, \overline{u_1(B)^2} \, \overline{\eta(R)^2} \, <S_z> \qquad (64)$$

where we have appropriately averaged values of $u_1(B)$ and $\eta(R)$. Since $u_1(B)$ is the wave function of the unperturbed alkali valence electronic orbital, $2\pi \overline{d}^3 \, \overline{u_1(B)^2}$ is of order unity.

We note in Eq. (64) that the value of ΔH for different isotopes of the same noble gas atom is the same for the same alkali polarization environment (neglecting a small effect of the different nuclear structure), but that different noble gas species experience different magnetic field shifts, mainly due to the different values of the exchange enchancement factor, η.

If we pick $\langle S_z \rangle \sim 0.1$ and a sample temperature of $65^\circ C$, we find the magnetic field shifts for Kr and Xe due to the presence of Rb as:

$$\Delta H_{Kr} \sim 2.6 \ \mu G, \text{ and}$$

$$\Delta H_{Xe} \sim 5.7 \ \mu G \ . \tag{65}$$

Under the present mechanization of Litton's NMR gyro, the gyro bias shift, Ω_a, due to the magnetic fields seen by the noble gas atoms is shown to be[8]:

$$\Omega_a = \frac{\gamma_b}{\frac{\gamma_b}{\gamma_a} - 1} \ (\Delta H_a - \Delta H_b) \tag{66}$$

where the subscripts a and b refer to the two nuclear species to be used in the sample, and the γ's are the corresponding nuclear gyro magnetic ratios. When the results of Eq. (65) are used, the gyro bias shift becomes 580 deg/hr. Samples that contain a pair of isotopic nuclei of the same noble gas atom, such as Xe^{129} and Xe^{131}, will show essentially zero bias shift since the factor $(\Delta H_a - \Delta H_b)$ is diminished.

In an NMR gyro, this gyro bias shift should not be a problem as long as it remained constant. Eq. (64) indicates, however, the gyro bias shift will vary as a function of the cell temperature (temperature sensitivity) or of the alkali-pumping light intensity. These shifts can be clearly deduced by noting that a change of the cell temperature will result in a change of both

the density of alkali atoms, N_A, and the alkali-polarization, S_z, and that a variation of the pumping light intensity at a fixed temperature will result in a variation of $<S_z>$. It is for this reason that two nuclear isotopes of the same noble gas atoms, i.e. Xe^{129} and Xe^{131}, are the preferred embodiment in the Litton approach to the development of an NMR gyro.

3.2.2 Frequency Shift in a Pair of Isotopic Nuclei of the Same Noble Gas

We have argued in the previous section that, when the spin exchange is dominated by binary type collisions, a pair of iso-topic nuclei of the same noble gas atom experiences the same fre-quency shifts, which results in a "zero" gyro bias shift. Inter-actions other than the dipolar spin-exchange process that may lead to a frequency shift are discussed in the following.

Nuclear Structure Effect

There will be a limit to the condition that a pair of isotopic nuclei of the same noble gas atom experiences the same frequency shift. This is due to the isotopic "hyperfine anomaly" resulting from nuclear structure effects, which makes the strength of the hyperfine interaction, $\gamma(R)$, not strictly the same for each mem-ber of the pair. Nevertheless, the departure due to this effect of the small variance in the gyromagnetic ratios of the pair[6] is never more than one part in 10^3.

Effect of Molecular Formation

It has been shown previously[7,9] that, in addition to the binary collisions, the spin exchange takes place through the formation of weakly-bound molecules, such as Rb-Xe, in the presence of a

third colliding body, such as N_2 buffer gas (three body collisions).
If the duration of the interaction is taken to be the duration of
the three body collision, τ_c, the magnetic field experienced by
the noble gas nuclei due to the formation of molecules, ΔH_{mole}, is
shown to be[6]:

$$\Delta H_{mole} = \frac{1}{g_N \mu_N} \left(\frac{1}{T_F} \right) \frac{\gamma_{ave} \tau_c}{1 + \gamma_{ave}^2 \tau_c^2} \langle S_z \rangle \qquad (67)$$

where T_F is the molecular formation rate, and both T_F and τ_c are
functions of the buffer gas density. It remains to be investi-
gated if the interaction strength and the collision time are the
same for different isotopes of the same noble gas under conditions
of identical buffer gas density.

Effect of Nuclear Quadrupole Moment

Consider the nucleus of Xe^{131} ($\vec{I} = 3/2$), the nuclear quadrupole
moment of which interacts with the electric field gradient at the
nuclear site. It has been stated in Section II that the electric
field gradient arises from deformation of the otherwise spherical
electronic shells of the zenon atom during inelastic collisions
with the cell walls. (The quadrupole interaction is absent in the
nucleus of Xe^{129}, because $\vec{I} = 1/2$.) The quadrupole interaction
of the noble gas nucleus is modeled as $2I$ oscillators, namely
3 oscillators for Xe^{131}, each with a single frequency. The
frequencies are dependent on the orientation of the cell with
respect to the magnetic field. When a cell, where the nuclear

quadrupole interaction is made cylindrically symmetric, is
oriented to the 'magic' angle, the three oscillator frequencies
become nearly identical to the frequency, ω_c, given by Eq. (23a):

$$\omega_c = \omega + \frac{54b^2\bar{\alpha}^2}{\omega} \qquad (68a)$$

where
$$\omega = -\gamma hH \qquad (68b)$$

$$b = \sin\theta \cos\theta \quad . \qquad (68c)$$

where ω is the unperturbed nuclear precession frequency in a
magnetic field H, and θ is the angle between the magnetic field
axis and the axis of cylindrical symmetry. The strength of the
quadrupole interaction, $\bar{\alpha}$, has been shown to be:

$$\bar{\alpha} = \left(\frac{\tau_s}{\tau_s + \tau_v}\right) \frac{e^2 Qq}{4I(2I-1)} \qquad (69)$$

where eq and eQ are the electric field gradient and the nuclear
quadrupole moment, respectively, as described in Section II.
τ_s is the sticking time of xenon atoms on the cell walls, and
τ_v is the time between wall collisions.

Any departure of the nuclear precessional frequency, ω_c, from the
unperturbed frequency, ω, results in the frequency shift. The
shift is seen from Eq. (68a) to be proportional to the square
of the strength of the nuclear quadrupole interaction. In a
high magnetic field (ω is large), however, this frequency shift
could be made relatively small. Discussions so far have been
limited to the first order effect of the nuclear quadrupole inter-
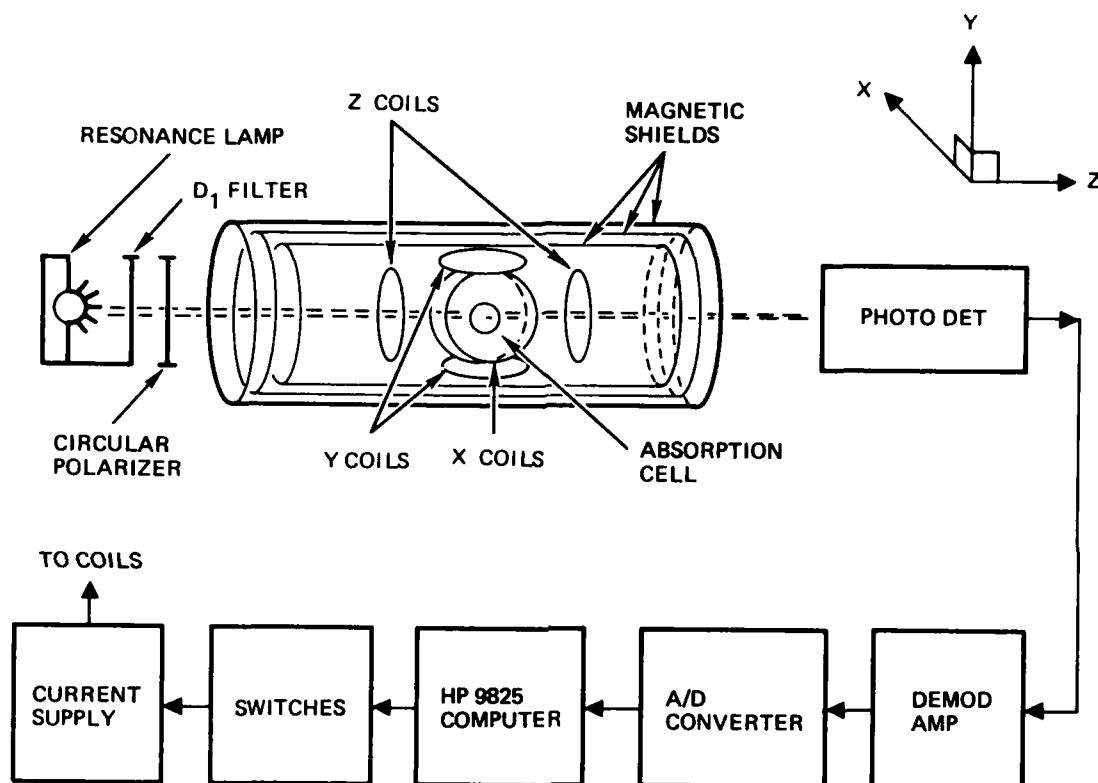action. The second order effects are small and are neglected.

3.3 EXPERIMENT

3.3.1 Description of Experiment

Shown in figure 6 is the experimental arrangement designed to measure the magnetic field experienced by the noble gas nucleus due to the spin exchange interaction with an optically oriented alkali vapor. This setup has been described in detail elsewhere[7]. Modifications of the arrangement are made so that the alkali pumping light beam can be made left or right hand circularly polarized by placing suitable polarizers in front of the light source. The left and right hand circular polarizers are made by laminating a sheet of plastic linear polarizer and two sheets of plastic retarder. The two polarizers so made transmit nearly equal intensity of rubidium D_1 light. The amount of circularly polarized light was measured to be 92% for one and 96% for the other of the transmitted light.

The experiments were performed by, first, polarizing the noble gas nuclear spins through spin exchange collisions with the optically oriented rubidium vapor (Pump Mode). The rubidium atoms were oriented by the absorption of left or right hand circularly polarized rubidium D_1 light in a standard longitudinal pumping scheme: This configuration is shown in figure 7(a). The pumping takes place in the presence of a longitudinal magnetic field (Pump Field) of approximately 100 mG along the z-axis. The longitudinal noble gas polarization, I_z, has been shown to obey the usual pumping law, given the initial condition $\langle I_z(t=0) \rangle = \langle I_z^0 \rangle$:

$$\langle I_z(t) \rangle = \langle I_z^0 \rangle \left\{ 1 - \exp(-t/T_p) \right\} \tag{70}$$

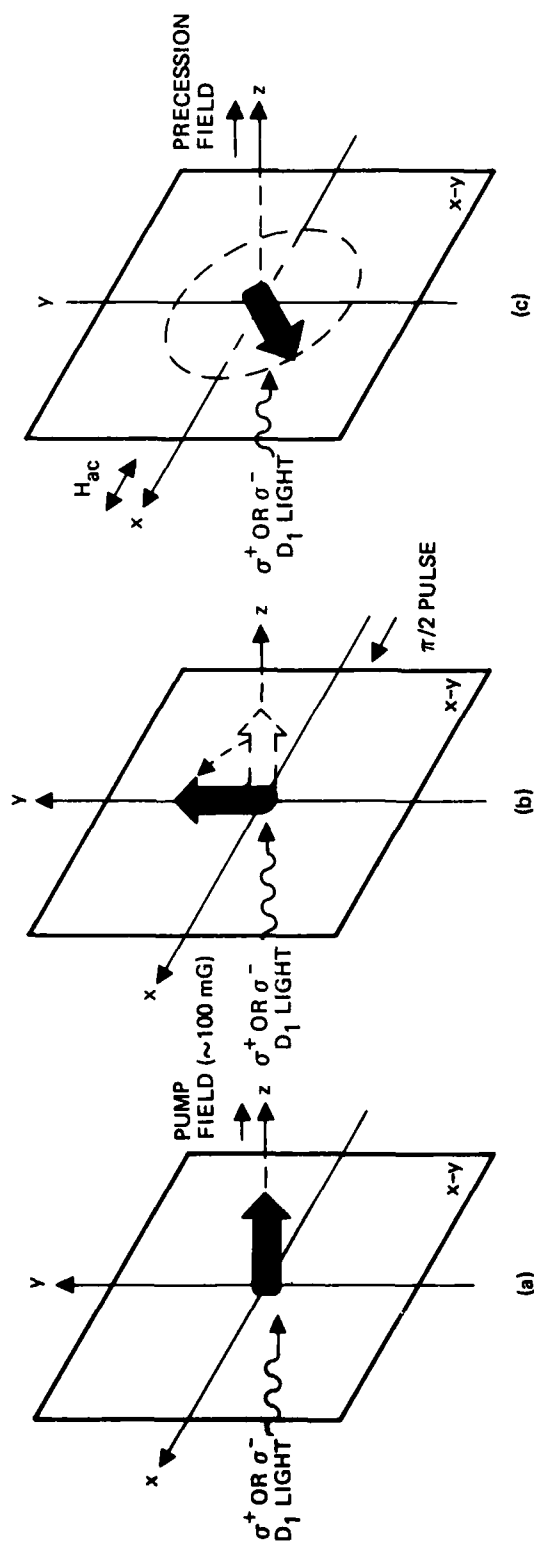Figure 6. Schematic representation of the experimental apparatus

Figure 7. Magnetic field arrangement for (a) the longitudinal pumping of the noble gas nuclear spin polarization, (b) application of $\pi/2$ pulse, and (c) the precession of the polarized nuclear spins. For brevity, only one species of noble gas nuclear moment is shown (thick arrow).

where T_p is the "pumping" time of the ensemble of noble gas
nuclear spins. The ensemble was pumped for a time sufficient to
build up a significant polarization. This time can range from
5 minutes at low sample temperatures to 30 minutes at high sample
temperatures.

When a sufficient nuclear polarization was built up along the
light beam axis (z-axis), the pump field was turned off, and, at
the same time, a "classic" $\pi/2$ pulse was applied along the x-axis
to the nuclear system. This "steers" the nuclear polarization
away from the z-axis into the x-y plane as shown in figure 7(b).

Finally, the precession of the noble gas nuclear spin polariza-
tion about the z-axis was accomplished by applying a precession
field ($\sim100~\mu G$) along the z-axis, figure 7(c). The optically
oriented rubidium vapor in this scheme, then, acts either to
directly increase or decrease the effective precession field as
experienced by the noble gas ensemble, depending on the circular
polarizers used in the measurement.

The precession frequency of the ensemble of the noble gas nuclei
is, correspondingly, increased or decreased such that:

$$\omega_1 = -\gamma(H_o + \Delta H)$$

(71)

$$\omega_2 = -\gamma(H_o - \Delta H)$$

where H_o is the magnetic field applied externally along the pre-
cession axis and ΔH is the field experienced by the noble gas

ensemble due to the spin exchange interaction. γ is the nuclear gyromagnetic ratio of the noble gas atoms. The subscripts, 1 and 2, refer to the two different circular polarizers. From these, ΔH is readily obtained by measuring the precession frequencies, ω_1 and ω_2. A similar experimental arrangement has been employed previously by Balling, et al[1-3], for the measurement of frequency shifts of electrons interacting with the polarized alkali vapor through the spin exchange process.

In order to observe the precessing nuclear spin polarization signal, the rubidium vapor was mechanized as a magnetometer. The magnetometer detects magnetic field variations along the x-axis due to the precessing noble gas nuclear ensemble. The form of the observed signal has been shown to be[7]:

$$S_i = S_a \exp\left[-t/(T_2)_a\right]\sin(\omega_{ai} + \varphi_{ai})$$

$$+S_b \exp\left[-t/(T_2)_b\right]\sin(\omega_{bi} + \varphi_{bi}), \text{ for } i=1 \text{ and } 2 \tag{72}$$

where the subscripts a and b refer to each species of noble gas nuclear isotope present in the cell, and i refers to the condition that either a left or a right hand circularly polarized beam is used in the experiment. T_2's are the transverse relaxation times and φ's are the initial phases. Data are then analyzed utilizing a Kalman filter technique to obtain the nuclear precession frequencies.

The samples used in the measurements are all 1-ml spherical cells made of pyrex glass. The glass envelopes were baked overnight at $300^\circ C$ under high vacuum. After the bake, rubidium metal was

distilled in:o the cell, and, a pair of noble gas isotopes, Xe^{129} and Kr^{83}, or Xe^{129} and Xe^{131}, together with buffer gases such as N_2 and/or He, were filled into the cell. In order to minimize the uncertainties of the gas pressures in the sealed-off cells, each of the spherical cells was completely covered with thermal insulation while the cell stems were sealed with a working flame. The rubidium metal in the sealed cells was then carefully driven into the small region of the cell stem area. The cells so made were then "aged" in an oven at 80°C for no less than two weeks before the measurements.

3.3.2 Experimental Results and Discussions

The results are presented for the three different sample cells listed in Table I. Cells 1-44 and 1-48 are for the Xe^{129}-Kr^{83} pair and cell 1-75 is for the Xe^{129}-Xe^{131} pair.

In figure 8, the magnetic fields, ΔH, experienced by Xe^{129} and Kr^{83} in cells 1-44 and 1-48 due to the spin exchange interaction with the optically oriented rubidium vapor are shown as a function of the cell temperature. The functional form of temperature dependence of the magnetic field qualitatively confirms the theory discussed earlier. As the cell temperature increases, the rubidium number density, N_A, increases, and, at the same time, the rubidium polarization, $<S_z>$, decreases, with ΔH being a function of the product of the two, $N_A<S_z>$. The magnitude of ΔH experienced by Xe^{129} is larger than that by Kr^{83} at all temperatures in the same cell (i.e. the same rubidium polarization environment). This is the result of the different magnitudes of the enhancement factors $\left(\text{i.e.} \left| \eta_{Xe} \right| > \left| \eta_{Kr} \right| \right)$.

TABLE I. LIST OF SAMPLE CELLS USED IN THE EXPERIMENT

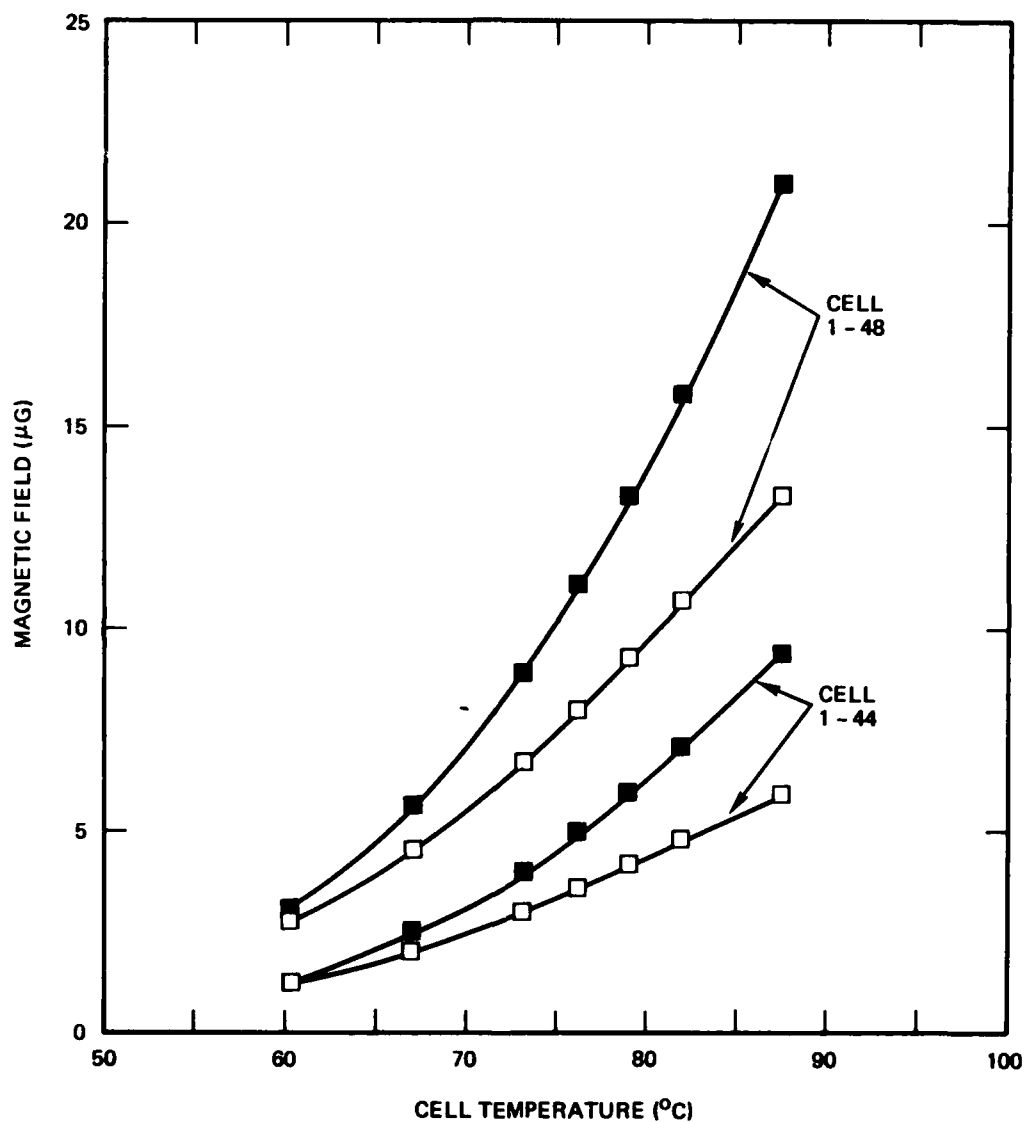| Cell S/N	Alkali Metal	Nuclear Species	Buffer
1 - 44	Rb^{87}	0.2 Torr of Xe^{129} and 5.0 Torr of Kr^{83}	15 Torr of N_2 and 140 Torr of He
1 - 48	Natural Rb	0.2 Torr of Xe^{129} and 5.0 Torr of Kr^{83}	100 Torr of N_2
1 - 75	Natural Rb	0.1 Torr of Xe^{129} and 0.4 Torr of Xe^{131}	10 Torr of N_2 and 100 Torr of He

Figure 8.   The magnetic fields experienced by Xe^{129}
(solid square) and Kr^{83} (empty square)
nuclei in two different sample cells as
a function of cell temperature

Comparing the magnitude of ΔH experienced by each isotope in the two different cells, the ones in cell 1-48 are larger than those in cell 1-44. This is understood to mean that higher N_2 pressure (100 torr) in cell 1-48 provides a higher degree of rubidium polarization than that provided in cell 1-44 (15 torr of N_2).

Attention is directed in figure 8 to the fact that the ratio of the magnetic field experienced by Xe^{129} to that by Kr^{83} due to the spin exchange is insensitive to the cell temperatures. The same ratio is observed within the experimental uncertainty even in the two different cells. This is an expected result from Eq. (64). The ratio determined by this measurement is 2.2 ± 0.1.

Essentially the same features are observed for cell 1-75, which is for the Xe^{129} and Xe^{131} pair, as shown in figure 9. The magnetic fields, ΔH, experienced by the two xenon isotopes are nearly identical at all temperatures. This confirms experimentally the theoretical argument presented earlier that, under the same alkali polarization environment, a pair of nuclear isotopes of the same noble gas would see nearly equal magnitudes of magnetic fields due to spin exchange with the optically oriented alkali vapor. The degree of the alkali polarization in cell 1-75 may be close to that in cell 1-44, in view of the fact that the magnitude of the magnetic fields experienced by Xe^{129} is nearly the same in the two cells.

The same data shown in figures 8 and 9 are presented in figures 10 and 11, respectively, in terms of NMR gyro bias shift as a function of temperature. Figure 10 shows $Kr^{83}-Xe^{129}$ cell bias shifts of -60 deg/hr and -100 deg/hr for a $1^{\circ}C$ variation of the cell temperature at a nominal cell operating temperature of $75^{\circ}C$ (temperature sensitivity).
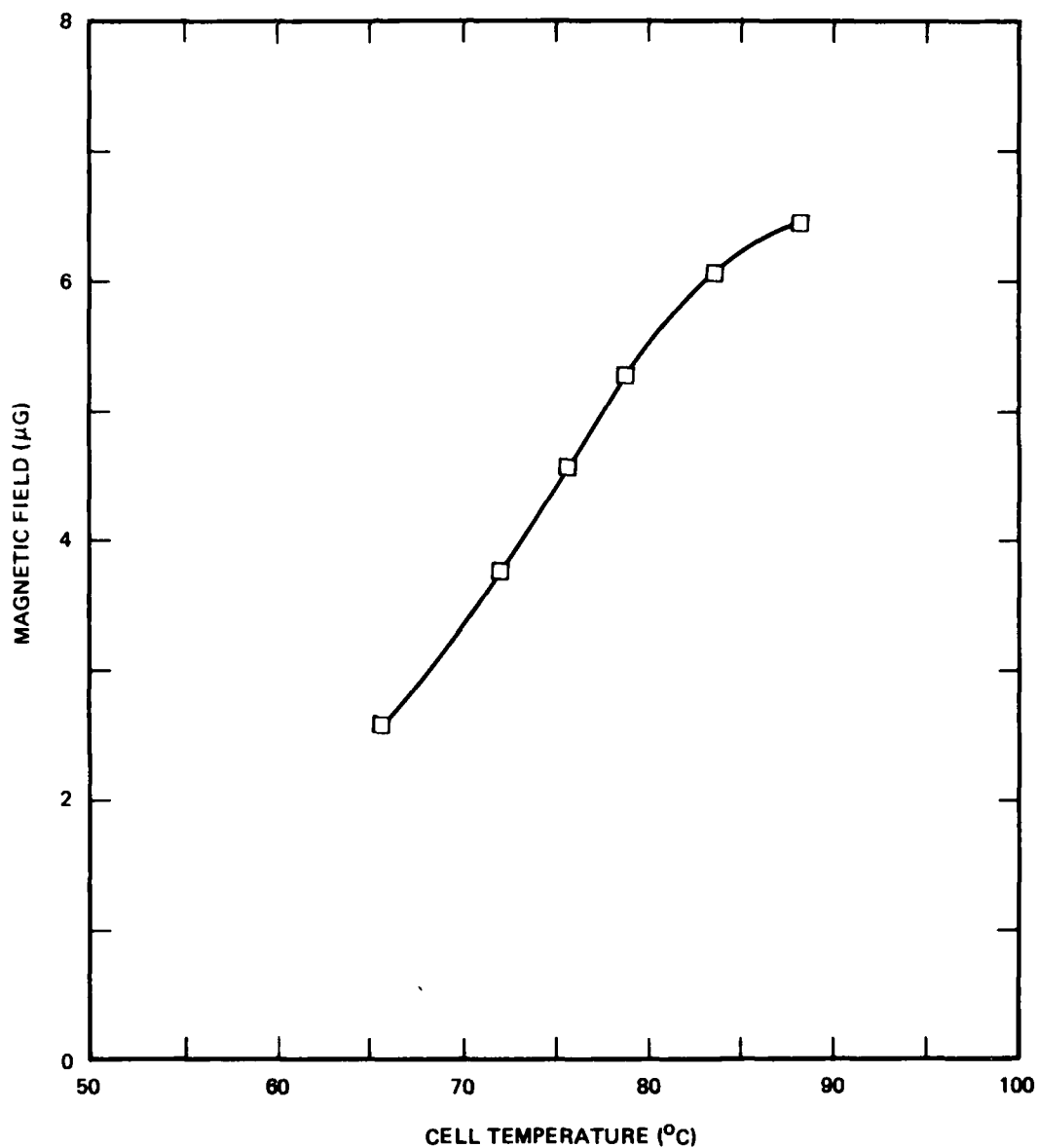
Figure 9. The magnetic fields experienced by both Xe^{129}
and Xe^{131} nuclei as a function of the sample
cell temperature. The difference of the
fields experienced by the two nuclear species
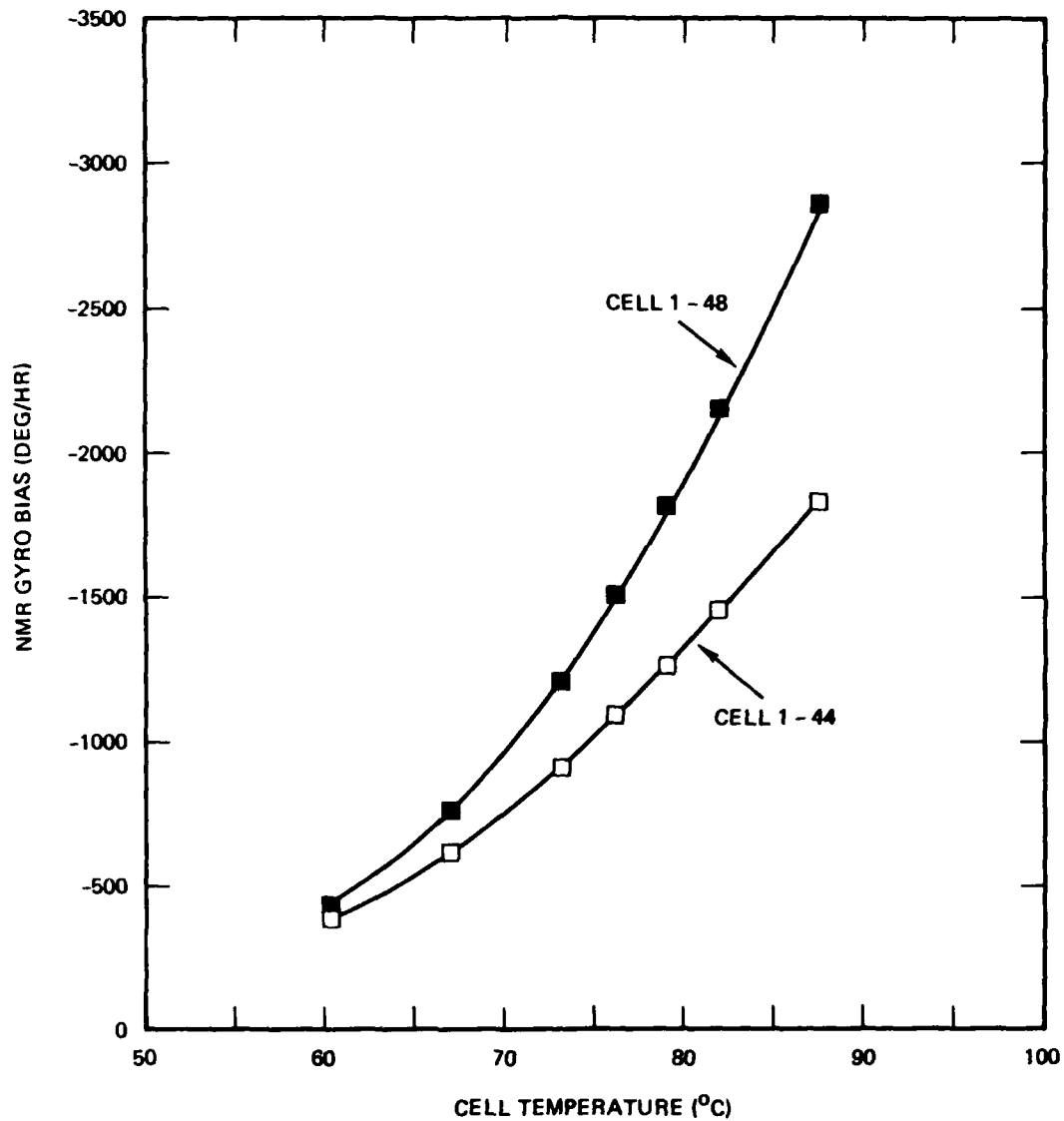are too small to be clearly seen in the plot.

Figure 10. NMR gyro bias versus the cell temperature for the cells with the Xe^{129} and Kr^{83} pair of isotopes. The same data shown in figure 3-3 are used.
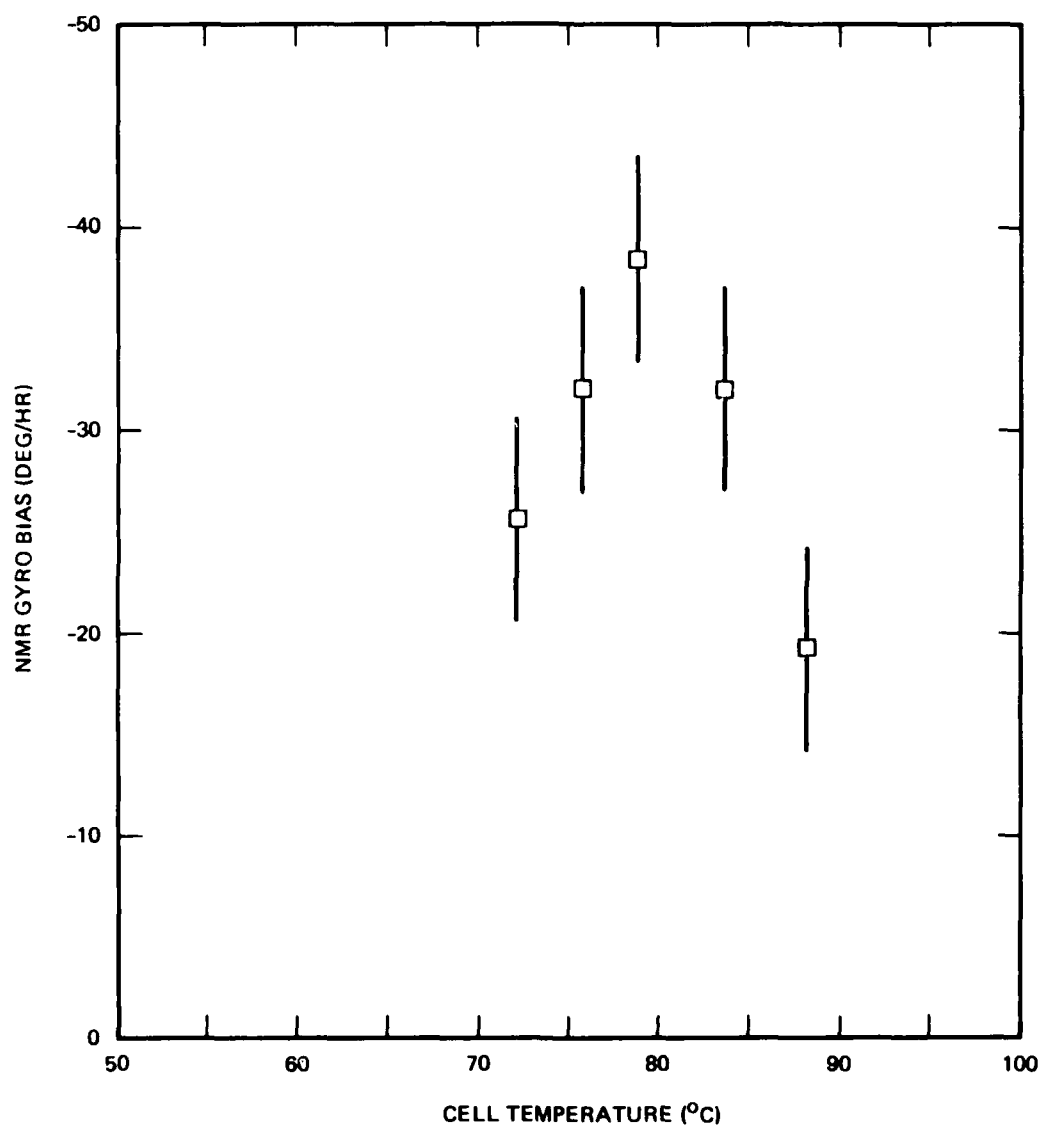
Figure 11. NMR gyro bias versus the cell temperature for the cell (1-75) with the Xe^{129} and Xe^{131} pair of isotopes. The same data shown in figure 3-4 are used. The large error bars are due to the computational error.

As shown in figure 11, the gyro bias shift in the cell with the Xe^{129} and Xe^{131} pair (cell 1-75) is at least an order of magnitude smaller than that in the cells with the Xe^{129} and Kr^{83} pair. The large error bars in figure 11 indicate the computation error. (Two nearly equal numbers have to be subtracted to get the gyro bias.) The existence of any gyro bias shift in this cell is not surprising in view of the discussions mentioned previously. (A few percent of this bias shift could have been caused by the different polarizabilities of the two circular polarizers used in the experiment.) Notice that, at $78^{\circ}C$, the bias becomes maximum, i.e., when the cell is operated at this temperature, sensitivity of the gyro bias will be identically zero.

3.4 SUMMARY AND FUTURE PLANS

A theory of nuclear precession frequency shift due to the spin exchange interaction with an optically oriented vapor was reviewed. Experimental results are qualitatively in good agreement with the theory. In particular, it has been confirmed experimentally that a pair of nuclear isotopes of the same noble gas atoms experience nearly equal frequency shifts under an identical alkali polarization environment.

The gyro bias shift in the cell with the Xe^{129} and Xe^{131} pair is at least an order of magnitude smaller than that of the cell with the Xe^{129} and Kr^{83} pair. It has been found in this work that there is a certain cell temperature, at which the temperature sensitivity of the gyro bias shift is identically zero. In order to possibly utilize the point of zero temperature sensitivity in an NMR gyro, the existence of any gyro bias shift

would have to be investigated further within the frame of the responsible physical phenomena discussed in the theoretical section. Some of the possible causes could be studied advantageously by varying the temperature of the cell wall while maintaining the product of alkali number density and the alkali polarization constant. This could be done in an experimental arrangement in which the wall and the cell tip (where the alkali metal reservoir is confined) temperatures are controlled separately.

3.5 BIBLIOGRAPHY FOR SECTION III

1. L. C. Balling, R. J. Hanson, and F. M. Pipkin, Phys. Rev. 133, A607 (1964)

2. L. C. Balling and F. M. Pipkin, Phys. Rev. 136, A46 (1964)

3. S. J. Davis and L. C. Balling, Phys. Rev. A6, 1479 (1972)

4. C. H. Volk, B. C. Grover, and E. Kanegsberg, AFOSR, Annual Technical Report (1978), Litton Document No. 403635 (unpublished)

5. R. H. Herman, Phys. Rev. 137, A1062 (1965)

6. F. G. Major, Litton Subcontract Report. Subcontract No. WC376807 (unpublished)

7. C. H. Volk, T. M. Kwon, and J. G. Mark, Phys. Rev. A21, 1549 (1980)

8. E. Kanegsberg and B. C. Grover, Naval Air Systems Command, Final Report, Contract No. N00019-78-C-0534 (1980) (unpublished)

9. N. D. Bhaskar, M. Hou, M. Ligare, B. Suleman, and W. Happer, Phys. Rev. A22, 2710 (1980)

10. C. H. Volk, T. M. Kwon, J. G. Mark, Y. B. Kim and J. C. Woo, Phys. Ref. Lett. 44, 136 (1980)

END

DATE
FILMED

7-81

DTIC